Eigenpolarization Theory of Monolithic Nonplanar Ring Oscillators

ALAN C. NILSSON, ERIC K. GUSTAFSON, AND ROBERT L. BYER, FELLOW, IEEE

Abstract—**Diode-laser-pumped monolithic nonplanar ring oscillators (NPRO's) in an applied magnetic field can operate as unidirectional traveling-wave lasers. The diode laser pumping, monolithic construction, and unidirectional oscillation lead to narrow linewidth radiation. In this paper, we present a comprehensive theory of the eigenpolarizations of a monolithic NPRO. We explain how the properties of the integral optical diode that forces unidirectional operation depend on the choice of the gain medium, the applied magnetic field, the output coupler, and the geometry of the nonplanar ring light path. Using optical equivalence theorems to gain insight into the polarization characteristics of the NPRO, we offer a strategy for designing NPRO's with low thresholds and large loss nonreciprocities. We present an analysis of the eigenpolarizations for one such NPRO, consider alternative optimization approaches, and discuss briefly the prospects for further reducing the linewidths of these lasers.**

I. Introduction

Nd:YAG lasers emitting frequency stable, narrow linewidth radiation have long been sought for applications such as coherent communication, injection locking, spectroscopy, remote sensing, and precision metrology. Technical noise has made it difficult to achieve laser linewidths narrower than several hundred kilohertz [1]–[3]. The recent invention of the monolithic nonplanar ring oscillator (NPRO) [4], [5], a diode-laser-pumped ring laser with an integral optical diode [6] that forces unidirectional traveling-wave operation, has overcome several technical noise problems. The principal sources of linewidth broadening and frequency instability in Nd:YAG lasers [7] are: 1) fluctuations in optical path length caused by vibration and temperature instabilities, 2) fluctuations caused by unstable optical pumping, 3) multiaxial mode oscillation caused by spatial hole burning, and 4) instability induced by extracavity optical feedback. The NPRO, by virtue of its diode-laser-pumped monolithic ring design, overcomes these four limitations.

First, the NPRO resonator is small ($5 \times 4 \times 2$ mm^3 for our recent designs) and rigid since it consists of a monolithic block of Nd:YAG or a similar material. Second, diode laser pumping can be extremely stable in both wavelength and power, and diode laser pumping greatly reduces the thermal loading of the resonator compared to lamp pumping [8]. Third, the integral optical diode forces unidirectional traveling-wave operation of the laser and thereby eliminates spatial hole burning, so the laser oscillates in a single axial mode. By properly focusing the diode laser pump radiation into the mode volume of the NPRO, TEM_{00} transverse mode operation is obtained as well. Fourth, the ring geometry reduces the sensitivity of the laser to extracavity optical feedback because output radiation reflected back into the NPRO cavity arrives in a high loss polarization state for its direction of propagation and is also frequency shifted from the resonant frequency for that direction (see Section II). Thus, the reflected light does not strongly couple to the oscillating mode.

Heterodyne experiments performed with a pair of free-running, diode-laser-array-pumped Nd:YAG NPRO's have demonstrated that the short-term linewidth of the output radiation can be as narrow as 3 kHz under favorable environmental conditions [9]. Recently, NPRO's with single-stripe diode laser pumps [10], [11] have been investigated, and these lasers may have even narrower linewidths.

The key to the operation of the NPRO as a unidirectional traveling wave laser is its integral optical diode. Discrete-element Faraday effect optical diodes have long been used to enforce stable unidirectional operation of solid-state [12]–[14], He-Ne [15], and ring dye lasers [16], [17]. The optical diode creates a polarization-dependent difference in loss for the eigenmodes of the two directions of propagation around a ring. The loss difference is produced by a combination of a reciprocal polarization rotator such as *c*-axis quartz, a nonreciprocal rotator such as a Faraday rotator, and a polarizer. Ideally, one arranges the reciprocal and nonreciprocal rotations to cancel for one direction of propagation and to add for the other. For the direction in which the rotations cancel, the eigenpolarizations are the low and high loss linear polarization states aligned with the principal axes of the partial polarizer. For the direction in which the rotations add, the eigenpolarizations are in general linear or elliptical polarization states with losses intermediate between the maximum and minimum possible values.

The NPRO combines the elements of the optical diode in the monolithic solid-state gain medium itself.[1] The

Manuscript received March 7, 1988; revised October 11, 1988. This work was supported by NASA Langley Contract NAG-1-839, Boeing Contract LC9712, and Hoya Optics, Inc.

The authors are with Edward L. Ginzton Laboratory, Stanford University, Stanford, CA 94305.

IEEE Log Number 8826324.

[1]It is interesting to note that Clobes and Brienza [13] obtained unidirectional oscillation in a discrete element ring in which the Nd:YAG laser rod alone served as the differential loss element. A magnetic field applied to the rod provided Faraday rotation. Thermally induced stress birefringence caused by pumping the rod with a 1500 W tungsten lamp served as the reciprocal waveplate. Brewster-angled endfaces on the rod served as the partial polarizer. The mirrors of the resonator served only to define a ring path for the light and to provide output coupling.

NPRO uses a four-reflector nonplanar ring resonator as its reciprocal polarization rotator [18]–[20]. (See also Appendix A.) A magnetic field applied to the gain medium causes nonreciprocal Faraday rotation. A multilayer dielectric mirror used at oblique incidence is the partial polarizer. The NPRO is a unidirectional ring laser with no discrete intracavity elements, which means that the resonator can have low internal loss and small intracavity coupling of counterpropagating modes. Fig. 1 shows a schematic of the diode laser pump and the monolithic Nd:YAG resonator with its nonplanar ring light path. The small permanent magnet shown in Fig. 1 applies a magnetic field to the Nd:YAG crystal to force unidirectional oscillation as shown.

In this paper, we present a comprehensive formalism for analyzing the eigenpolarizations of a monolithic NPRO. We explain how the properties of the integral optical diode depend on the choice of the gain medium, the applied magnetic field, the geometry of the nonplanar ring light path, and the output coupler. Using optical equivalence theorems to gain insight into the behavior of the NPRO, we discuss a design strategy for producing low threshold devices with strong intracavity optical diodes. We conclude with a detailed analysis of the eigenpolarizations for one such NPRO, and we discuss the prospects for further reducing the linewidths of these unique lasers.

II. Theory of the NPRO

We present in this section the eigenpolarization theory for a monolithic, optically isotropic, nonplanar ring laser based on the Jones matrix calculus. Extensive discussion of the Jones calculus can be found in Jones's original papers [21], [22] and in Azzam and Bashara [23]. Applications of the Jones calculus to finding eigenpolarizations of anisotropic laser resonators are found in [24]–[32] and references therein. In this section, we first review the Jones calculus, describe the geometry of the light path in the nonplanar ring, and introduce the coordinate systems used in our analysis. Then we give the explicit forms of the Jones matrices for the polarization-influencing elements of the resonator, and we find the round trip Jones matrices for the two directions of propagation around the ring. From the round trip matrices we solve for the eigenvalues, from which we derive the round trip losses and the frequency differences of the polarization eigenmodes. We conclude with a brief discussion of the eigenpolarizations themselves and a description of the parameters used to specify the NPRO.

A. Review of Jones Matrix Calculus

Consider a monochromatic TEM plane wave propagating along the z axis in a lossless, isotropic medium. The polarization of the light at a point in space is defined by the behavior of the electric field $\boldsymbol{E}$ at that point as a function of time. For a uniform plane wave we write the electric field as

$$\boldsymbol{E}(z, t) = \mathrm{Re}\left\{\boldsymbol{E}_0 \exp\left[i(\omega t + \phi)\right] \exp\left(-ikz\right)\right\}. \quad (1)$$

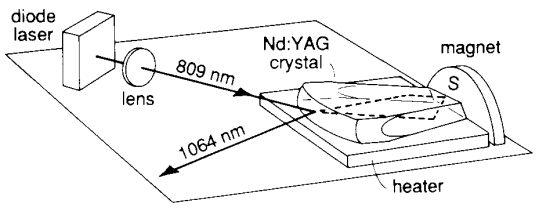

Fig. 1. Schematic of diode-laser-pumped monolithic nonplanar ring oscillator (NPRO). The laser operates unidirectionally because the combination of the nonplanar ring light path in the crystal, the Faraday rotation caused by the applied magnetic field, and the oblique angle of incidence on the output coupler produces a loss difference between the two directions of propagation around the ring.

Here $\boldsymbol{E}_0$ is a complex vector amplitude, $\boldsymbol{E}_0 = E_x\hat{\boldsymbol{x}} + E_y\hat{\boldsymbol{y}}$ where E_x and E_y are complex.

The Cartesian Jones vector (the Jones vector expressed with respect to the linear polarization basis states $\hat{\boldsymbol{x}}$ and $\hat{\boldsymbol{y}}$) for the above electric field contains the information on the state of polarization and suppresses the propagation terms. The Cartesian Jones vector $\boldsymbol{E}$ is given by [23]

$$\boldsymbol{E} = \begin{bmatrix} E_x \\ E_y \end{bmatrix}. \quad (2)$$

Unless one is interested in the amplitude and absolute phase of the electric field, it suffices to characterize the state of polarization by the ratio of the components of the Jones vector,

$$\chi = \frac{E_y}{E_x} = \frac{|E_y|}{|E_x|} e^{i\delta} \quad (3)$$

with $\delta = \arg(E_y) - \arg(E_x)$.

From the complex number χ we find the azimuth θ $(-\pi/2 \le \theta < \pi/2)$, and ellipticity parameter ϵ $(-\pi/4 \le \epsilon \le \pi/4)$ of the elliptical polarization state by

$$\tan(2\theta) = \frac{2\,\mathrm{Re}(\chi)}{1 - |\chi|^2} \quad (4)$$

$$\sin(2\epsilon) = \frac{2\,\mathrm{Im}(\chi)}{1 + |\chi|^2}. \quad (5)$$

The azimuth is the acute angle between the major axis of the ellipse and the x axis of the coordinate system. Let the semimajor (semiminor) axis of the ellipse be $a(b)$. The ratio of the axes b/a where $0 \le b/a \le 1$ is called the ellipticity. The helicity of the elliptically polarized light is the sign of the projection of the angular momentum of the light onto the direction of propagation. Helicity relates to the sense in which the ellipse is traced in time by the electric field vector. If the ellipse is traced in the counterclockwise (clockwise) sense as seen by an observer looking toward the light source, the helicity is positive (negative). Thus, positive helicity corresponds to the traditional optics convention for left-handed light, and negative helicity corresponds to right-handed light. The helicity and the ellipticity are combined into a single ellipticity parameter ϵ such that $|\tan(\epsilon)| = b/a$, with ϵ

positive for right-handed light and negative for left-handed light.

The Jones matrix of an optical element is the 2 × 2 complex matrix M that maps the input Jones vector into the output Jones vector, that is

$$\begin{bmatrix} E_x \\ E_y \end{bmatrix}_{\text{out}} = \begin{bmatrix} M_{11} & M_{12} \\ M_{21} & M_{22} \end{bmatrix} \begin{bmatrix} E_x \\ E_y \end{bmatrix}_{\text{in}}. \tag{6}$$

The Jones matrix calculus is straightforward mathematically, but there are many pitfalls involving polarization conventions, coordinate system conventions, and forms of the Jones matrices themselves. We have adopted the polarization conventions recommended by Bennett and Bennett in the *Handbook of Optics* [33] and used by Azzam and Bashara [23]. We will exhibit our coordinate systems and the explicit forms of the Jones matrices as we proceed.

B. Geometry of Light Path

A general NPRO resonator is shown in top and side views in Fig. 2. The monolithic, nonplanar ring resonator is a single block of optically isotropic gain medium (e.g., Nd:YAG) with a ring path defined by four reflecting surfaces whose normals are not coplanar. The facets containing points B, C, and D are optically polished flat surfaces at which total internal reflection (TIR) occurs. The output coupler at A is a convex spherical surface with a multilayer dielectric mirror coating that is partially transmitting. The curvature of the surface at A determines the properties of the spatial modes of the resonator.

The ray geometry of the light path within the resonator is shown in Fig. 3. Fig. 3(a) shows the light path with unit propagation vectors along each leg, and (b) introduces the notation for the angles that specify the light path. The light path is the perimeter of a three-dimensional geometric figure formed by joining two isosceles triangles (ABD and BCD) along a common base (BD). The dihedral angle between the two planes of the triangles is denoted by β. For any value of β other than 0 or π, the light path is nonplanar. The light path has a plane of reflection symmetry (ACE). A uniform magnetic field $\boldsymbol{B}$ is applied parallel to AE as shown in Fig. 3(b). We denote the angles of incidence at A, B, C, and D by θ_A, θ_B, θ_C, and θ_D ($= \theta_B$), respectively.

The geometry of the light path has four degrees of freedom: two parameters for the first isosceles triangle, a single parameter for the second isosceles triangle (since the triangles share a common base), and one parameter to characterize the nonplanarity. The light path is fully specified by, for example, the lengths AE and CE of the isosceles triangles, together with the two angles θ_A and β. We choose these parameters due to their physical significance. The angle of incidence on the output coupler θ_A determines both the astigmatism of the resonator and the difference between the s and p Fresnel reflection coefficients. The dihedral angle β measures the nonplanarity of the resonator. The length AE determines the amount of

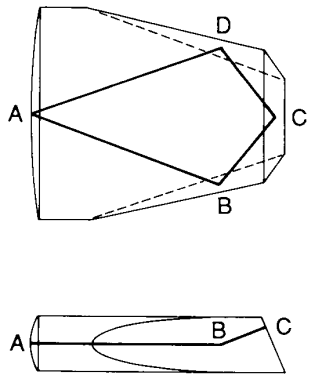

Fig. 2. Top and side views of the monolithic laser crystal with the nonplanar ring light path indicated (bold line). Total internal reflection occurs at B, C, and D. Output coupling occurs at A, a partially transmitting, multilayer dielectric coated spherical surface.

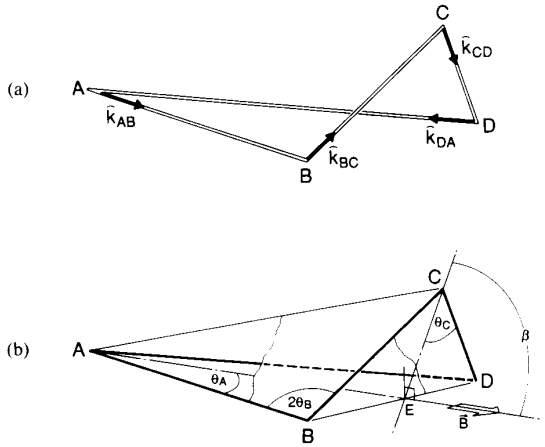

Fig. 3. (a) A perspective view of the nonplanar ring light path with unit propagation vectors for CCW propagation shown on each leg. (b) Notation for characterizing the nonplanar ring. The angles of incidence at A, B, C, and D are θ_A, θ_B, θ_C, and θ_D ($= \theta_B$), respectively. The dihedral angle β characterizes the nonplanarity: it is the angle between planes ABD and BCD. Point E is an auxiliary point useful in defining lengths and directions in the ring, because plane AEC is a plane of mirror symmetry for the geometry. An external magnetic field $\boldsymbol{B}$ is applied parallel to AE.

Faraday rotation that occurs along legs AB and DA since AE is the projection of those legs parallel to the applied magnetic field. Similarly, $CE\cos(\beta)$ determines the amount of Faraday rotation that occurs along legs BC and CD.

C. Coordinate System Conventions

There are two ways to traverse the ring: counterclockwise (CCW) and clockwise (CW) as viewed from above the light path (upper view of Fig. 2). Fig. 3(a) shows the unit vectors for propagation along each leg in the CCW direction $A \rightarrow B \rightarrow C \rightarrow D \rightarrow A$. In Figs. 4 and 5 we introduce the coordinate systems used in analyzing CCW propagation. There are four reflections in a round trip through the resonator. We describe the incident and reflected waves in the principal axis system (basis vectors

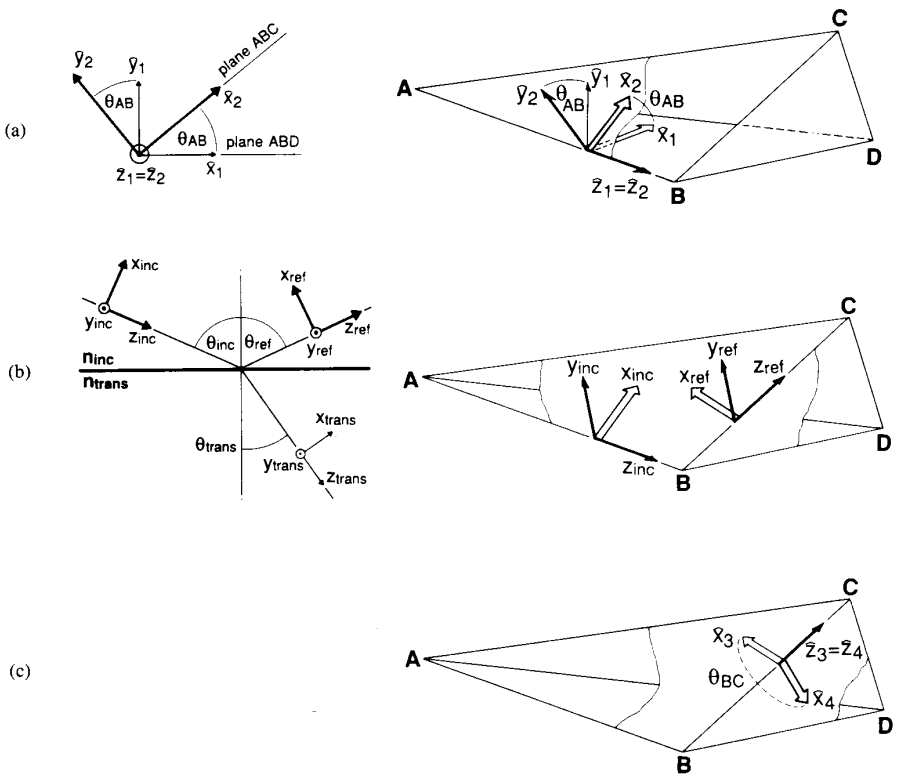

Fig. 4. (a) The two coordinate systems used for describing propagation of light along leg AB are related by a rotation about AB. The figure on the left is drawn from the point of view of an observer at B looking toward A, and the figure on the right is a perspective view. Positive rotation of system 1 by θ_{AB} rotates the normal to the plane of incidence at A, $\hat{y}_1$, into the normal to the plane of incidence at B, $\hat{y}_2$. (b) Two views of the coordinate systems used to describe reflection from a planar interface between two isotropic media. The figure on the left is used in defining the phases of the Fresnel coefficients. The figure on the right shows a perspective view of the two coordinate systems associated with a total internal reflection at B. (c) To transform from the principal axis system for reflection at B into the principal axis system for reflection at C requires a negative rotation about axis BC through the angle θ_{BC} as shown here. For simplicity only the basis vectors in the two planes of incidence are shown.

perpendicular and parallel to the plane of incidence) for the given reflector. Since the resonator is nonplanar, the planes of incidence for successive reflections do not coincide. For example, to transform from the principal axis system for reflection at A into the principal axis system for reflection at B requires a rotation about the axis AB by the angle θ_{AB}, which is the dihedral angle between planes ABD and ABC. We show two views of this transformation in Fig. 4(a). The left-hand side of Fig. 4(a) is drawn from the point of view of an observer at B looking toward A, and the right-hand side is a perspective view.

There are many different conventions for the coordinate systems used to describe reflection, and the phases of the Fresnel coefficients depend on the coordinate systems. Our coordinate systems are shown on the left in Fig. 4(b). The orthogonal unit vectors for the incident and reflected coordinate systems are chosen as follows. Set $\hat{z}$ parallel to the propagation direction $\hat{k}$. Choose $\hat{y}$ perpendicular to the plane of incidence and common to both coordinate systems, and choose $\hat{x}$ in the plane of incidence such that $\hat{x} \times \hat{y} = \hat{z}$. The incident and reflected coordinate systems thus share a common $\hat{y}$ and are related by a rotation about $\hat{y}$ through an angle $\pi - 2\theta_{\text{inc}}$ where θ_{inc} denotes the angle of incidence. In this set of coordinate systems, the complex Fresnel amplitude coefficients for reflection from a planar interface between two nonmagnetic, lossless, optically isotropic media are [34]

$$\tilde{r}_s = \frac{E_y(\text{ref})}{E_y(\text{inc})} = \frac{-\sin(\theta_{\text{inc}} - \theta_{\text{trans}})}{\sin(\theta_{\text{inc}} + \theta_{\text{trans}})} \tag{7}$$

$$\tilde{r}_p = \frac{E_x(\text{ref})}{E_x(\text{inc})} = \frac{\tan(\theta_{\text{inc}} - \theta_{\text{trans}})}{\tan(\theta_{\text{inc}} + \theta_{\text{trans}})} \tag{8}$$

where subscripts s and p mean perpendicular and parallel to the plane of incidence, respectively; $E(\text{inc})$ and $E(\text{ref})$ are the incident and reflected electric field amplitudes, θ_{inc}

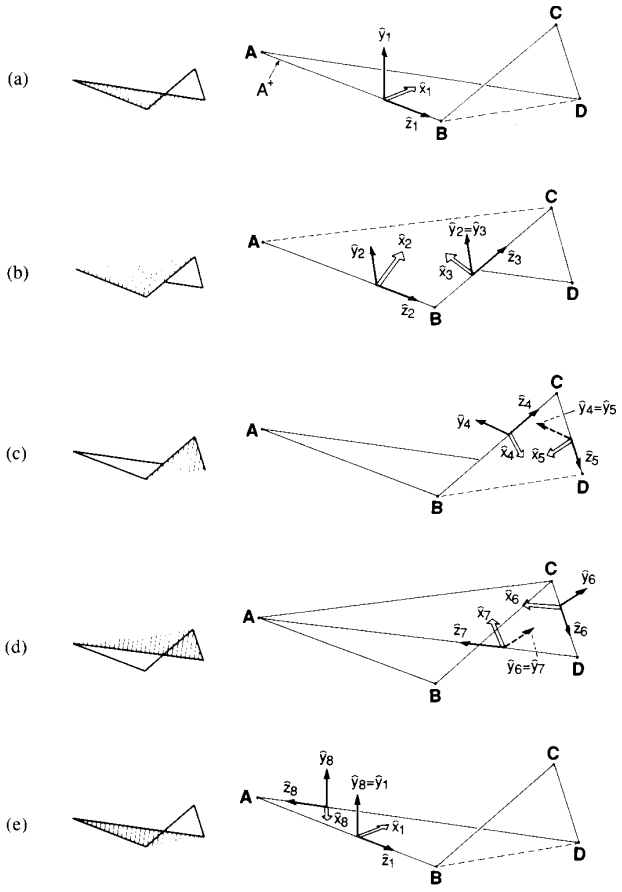

Fig. 5. Successive views of the nonplanar ring light path showing the eight coordinate systems used to describe counterclockwise propagation of light, beginning at the point labeled A^+ in (a). The successive planes of incidence are the shaded planes of the small figures on the left. The basis vectors are always chosen such that $\hat{x}$ is in a local plane of incidence, $\hat{y}$ is perpendicular to a local plane of incidence, and $\hat{z}$ is in the local direction of propagation.

is the angle of incidence, and θ_{trans} is the angle of refraction related to θ_{inc} by Snell's law. Note that θ_{trans} is complex for the case of total internal reflection.

The right-hand side of Fig. 4(b) shows a perspective view of the two coordinate systems associated with reflection from *B*. To describe reflection from *C*, we must once again rotate coordinate systems. Fig. 4(c) shows the rotation through θ_{BC} that moves $\hat{x}$ from the plane of incidence at ***B*** into the plane of incidence at *C*. Finally, Fig. 5 shows all of the coordinate systems for a round trip in the CCW direction. The shaded planes shown on the left of the figure are the successive planes of incidence for the reflections that define the light path. We begin our analysis of the CCW propagation at the point labeled A^+ in Fig. 5(a). Since there are two coordinate systems per reflection and four reflections in a round trip, we have eight different coordinate systems, labeled $1 \cdots 8$ in Fig. 5. The two coordinate systems associated with reflection at a vertex are related by rotation about their common $\hat{y}$, and along a given leg the two coordinate systems are related by a rotation about their common $\hat{z}$. Note that the $\hat{x}$ vectors in Fig. 5 lie in the indicated shaded planes, as described previously.

To obtain the coordinate systems used for analysis of the CW propagation, we simply rotate each of the local CCW coordinate systems by π about its y axis. This rotation places the local $\hat{z}$ along the new direction of propagation, preserves the choice of the perpendicular ($\hat{y}$) to the local plane of incidence, and reverses the direction of $\hat{x}$ to keep the coordinate system right handed.

The motivation for introducing this collection of 16 local coordinate systems is that they are the principal axis systems for the reflections, and the Jones matrices are most simply expressed in the principal axis coordinate systems. Additionally, the distinction between CCW and CW coordinate systems makes possible a simple proof of the need for the nonplanar geometry in establishing unidirectional operation (see Section II-F.1). We believe that these conventions best separate the physics of the problem from the complications of the nonplanar geometry.

D. Explicit Forms of Jones Matrices

We assume three properties for the solid-state gain medium from which the resonator is constructed: homogeneous broadening of the laser transition, optical isotropy, and Faraday rotation in an applied magnetic field. We further assume that the pumped medium is optically isotropic, i.e., we neglect the small thermal birefringence induced by the diode laser pumping, and we do not consider nonlinear saturation effects. Within a monolithic resonator made from such a medium (e.g., Nd:YAG, a cubic crystal with a nonzero Verdet constant), the polarization of light is modified by reflections and by propagation along an applied magnetic field. Thus, Jones matrices for reflection and rotation appear in our analysis. We express the Jones matrices for reflections in their principal axis systems, so those matrices are diagonal. Here we give, for each polarization-influencing effect in the resonator, the explicit Jones matrices for CCW (superscript +) and CW (superscript −) propagation.

1) Jones Matrices for Reflection from the Output Coupler at A: The Jones matrices for reflection from the output coupler at *A* are identical for CCW and CW propagation and are given by

$$M_A^+ = M_A^- = \begin{bmatrix} \tilde{r}_p & 0 \\ 0 & \tilde{r}_s \end{bmatrix} \tag{9}$$

where $\tilde{r}_p$ and $\tilde{r}_s$ are the Fresnel amplitude reflection coefficients for the mirror at *A*. These coefficients are complex numbers with unequal moduli due to the oblique angle of incidence on the dielectric mirror. We can extract and neglect any common phase factor from $\tilde{r}_s$ and $\tilde{r}_p$ and rewrite the matrix as

$$M_A^+ = M_A^- = \begin{bmatrix} r_p e^{i(\Delta/2)} & 0 \\ 0 & r_s e^{-i(\Delta/2)} \end{bmatrix} \tag{10}$$

where $r_p = |\tilde{r}_p|$, $r_s = |\tilde{r}_s|$, and Δ is the relative phase shift on reflection, defined by

$$\Delta = \delta_p - \delta_s. \tag{11}$$

In principle, the phase shift on reflection from a dielectric mirror can be calculated by the method of characteristic matrices [35]. The phase shift that occurs in practice will depend on the complicated details of the thin film coating process used to make the dielectric stack. Experimentally, therefore, one must measure the phase shift on reflection from a multilayer dielectric mirror ellipsometrically. For theoretical simplicity, our analysis assumes that a quarter-wave dielectric stack with the standard relative phase shift $\Delta = \pi$ is used. We assume that $r_s > r_p$ as is typical for high reflectors, and we factor out r_s from the Jones matrix to emphasize only the anisotropy. For such a reflector we can write the Jones matrix in the simpler form

$$M_A^+ = M_A^- = r_s \begin{bmatrix} i\rho & 0 \\ 0 & -i \end{bmatrix} \tag{12}$$

where we have introduced the parameter $\rho = r_p/r_s$ that characterizes the amplitude anisotropy of reflection from the output coupler.[2] Note that $\rho = 1$ implies equal reflection for s and p components, and $\rho = 0$ implies that the reflector only reflects the s component of incident light. We refer to the parameter ρ as the partial polarizer strength of the output coupler, with smaller ρ corresponding to a stronger polarizer. The Jones matrix for the output coupler with a relative phase shift $\Delta = \pi$ [(12)] is equal to the product of three terms: 1) the modulus of the amplitude reflection coefficient for s-polarized light r_s, 2) the Jones matrix for a linear partial polarizer with partial polarizer strength ρ,

$$\begin{bmatrix} \rho & 0 \\ 0 & 1 \end{bmatrix}$$

and 3) the Jones matrix for a half-wave plate,

$$\begin{bmatrix} i & 0 \\ 0 & -i \end{bmatrix}.$$

2) Jones Matrices for Total Internal Reflection (TIR) at B, C, and D: The Jones matrices for total internal reflection are identical in form to the Jones matrices for reflection from a dielectric mirror, except that the moduli r_p and r_s are both unity, and we have a simple formula for calculating the relative phase shift Δ. The Jones matrix for TIR at vertex $j = B$, C, or D is written as

$$M_j^+ = M_j^- = \begin{bmatrix} e^{i(\Delta_j/2)} & 0 \\ 0 & e^{-i(\Delta_j/2)} \end{bmatrix} \tag{13}$$

where the relative phase shift Δ_j is related to the index of refraction n and the angle of incidence θ_j by [36]

$$\tan\left(\frac{\Delta_j}{2}\right) = \frac{\cos(\theta_j)\sqrt{\sin^2(\theta_j) - \frac{1}{n^2}}}{\sin^2(\theta_j)}. \tag{14}$$

Here it is assumed that the external medium has an index of refraction equal to one. For a bare surface Δ is positive and lies in the range $0 \le \Delta \le \Delta_{\max}$, where the upper limit $\Delta_{\max} \le \pi$ depends on the index n according to $\tan(\Delta_{\max}/2) = (n^2 - 1)/2n$. The Jones matrix for TIR is identical in form to the Jones matrix for a lossless, linear birefringent waveplate. Indeed, Fresnel rhombs are examples of TIR-based retarders.

The angles of incidence at B, C, and D can be calculated in terms of the parameter set used to specify the geometry of the nonplanar ring light path, AE, CE, θ_A, and β. We give the relevant equations in Appendix B. The requirement that TIR occur at B, C, and D imposes restrictions on the permissible geometries for the light path because each of θ_B, θ_C, and θ_D must exceed the critical angle of incidence for the medium $\theta_{\text{crit}} = \sin^{-1}(1/n)$.

3) Matrices for Rotations of Coordinate Systems: Successive mirror reflections involve different principal axis systems related by rotation about their common $\hat{z}$. Since the Jones matrices are expressed in their principal axis systems, we must introduce rotation matrices for transformation of the Jones vector between successive principal axis systems. We write rotation matrices as

$$R(\alpha) = \begin{bmatrix} \cos(\alpha) & -\sin(\alpha) \\ \sin(\alpha) & \cos(\alpha) \end{bmatrix}. \tag{15}$$

The operator that projects a Jones vector into a new coordinate system related to the old one by a positive rotation of the coordinate axes about their common $\hat{z}$ by angle α is the rotation matrix $R(-\alpha)$. The minus sign appears on α because we write the rotation operator in the active sense: physically rotating the vector in the positive sense by α in a fixed coordinate system is represented by $R(\alpha)$. Consider the coordinate system transformations involved on leg AB. For CCW propagation (from A to B) we must rotate the CCW coordinate system at A by θ_{AB} in the positive sense about $\hat{k}_{AB}$ to get the CCW coordinate system at B [see Fig. 4(a)]. For CW propagation (from B to A) we must rotate the CW coordinate system at B also by θ_{AB} in the positive sense about $\hat{k}_{BA}$ to get the CW coordinate system at A. The sign of the required rotation angle does not change, because we use different coordinate systems for the two directions of propagation. Thus, we have for the changes of coordinate systems on a given leg joining vertex j to adjacent vertex k

$$R_{j\to k}^+(\theta_{jk}) = R_{k\to j}^-(\theta_{jk}). \tag{16}$$

Equations for calculating the two required coordinate system rotation angles θ_{AB} and θ_{BC} in terms of the ring parameters AE, CE, θ_A, and β are given in Appendix B.

4) Jones Matrices for Faraday Rotation: Light propagating in an otherwise optically isotropic medium in an

[2]Note that the parameter ρ defined here is the modulus of the usual ellipsometric parameter bearing the same symbol [23].

applied magnetic field experiences Faraday rotation. The azimuth of the polarization state is rotated by an angle

$$\gamma = VL\hat{\boldsymbol{k}} \cdot \boldsymbol{B} \tag{17}$$

in propagating a distance L in the medium. Here, V is the Verdet constant of the medium, $\hat{\boldsymbol{k}}$ is a unit vector in the direction of propagation, and $\boldsymbol{B}$ is the applied magnetic field. The corresponding Jones matrix is again a rotation matrix, given by

$$M = R(\gamma) = \begin{bmatrix} \cos(\gamma) & -\sin(\gamma) \\ \sin(\gamma) & \cos(\gamma) \end{bmatrix}. \tag{18}$$

Note that for a given V, L, and $\boldsymbol{B}$, the sign of the Faraday rotation angle depends on the direction of propagation with respect to the field $\boldsymbol{B}$. Consider propagation along a given leg, say AB, and assume the magnetic field is applied parallel to AE. Then for CCW propagation from A to B the Faraday rotation Jones matrix is $R(\gamma_{AB})$, whereas for CW propagation from B to A the sign of the angle changes because the direction of propagation $\hat{\boldsymbol{k}}$ has been reversed, and the Jones matrix is $R(-\gamma_{AB})$. Reversal of direction of propagation changes the signs of the Faraday rotation angles in our coordinate system convention but does not change the signs of the geometric rotation angles. This sign difference is the manifestation of the nonreciprocal nature of the Faraday effect. The physical direction of polarization rotation due to the Faraday effect is determined only by the direction of the magnetic field and does not depend on the direction of propagation. Coordinate systems and sign conventions enter into the determination of the algebraic signs of the Faraday rotation angles. Therefore,

$$M^{+}_{j\to k} = R(\gamma_{jk}) \tag{19a}$$

$$M^{-}_{k\to j} = R(\gamma_{kj}) = R(-\gamma_{jk}). \tag{19b}$$

By extracting common phase factors from the Fresnel amplitude reflection coefficients, we have expressed the Jones matrices for all but the reflection from the output coupler as two-dimensional unitary matrices with determinant $+1$, which defines these Jones matrices as members of the special unitary group SU_2. The output coupler's Jones matrix cannot be unitary in general because energy is lost through the output coupler, and the output coupler acts as a partial polarizer. The group properties of SU_2 are helpful both analytically and numerically since they reduce the work involved in evaluating and checking products. The most general element of SU_2 can be written in the form

$$U = \begin{bmatrix} a & -b^* \\ b & a^* \end{bmatrix} \tag{20}$$

with a and b complex numbers such that $(aa^* + bb^*) = 1$. In evaluating a product of two elements of SU_2 it thus suffices to find just the two entries of a row or column in order to know the entire matrix.

E. Round Trip Jones Matrices for CCW and CW Propagation

In steady-state laser operation, the polarization state at any point along the beam axis of the resonator must repeat itself after a round trip. We have assumed that the pumped medium is optically isotropic, so the main effect of the gain is to maintain the amplitude of the electric field. The allowed polarizations of the cavity are determined by the anisotropy of the unpumped cavity, so we will solve for the eigenpolarizations of the unpumped cavity. First, we must derive the expressions for the round trip Jones matrices in terms of the individual Jones matrices described in Section II-D.

A convenient starting point for the analysis is the point labeled A^+ in Fig. 5(a). The ring may be traversed in two ways starting from A^+. The CCW path $A^+ \to B \to C \to D \to A \to A^+$ is denoted by a superscript $(+)$. The CW path $A^+ \to A \to D \to C \to B \to A^+$ is denoted by a superscript $(-)$. The round trip Jones matrices for these two paths are

$$M^+ = M_A R(\theta_{AB} - \gamma_{AB})\, M_D R(-\theta_{BC} - \gamma_{BC}) \cdot M_C R(\theta_{BC} + \gamma_{BC})\, M_B R(-\theta_{AB} + \gamma_{AB}), \tag{21}$$

$$M^- = R(-\theta_{AB} - \gamma_{AB})\, M_B R(\theta_{BC} - \gamma_{BC}) \cdot M_C R(-\theta_{BC} + \gamma_{BC})\, M_D R(\theta_{AB} + \gamma_{AB}) M_A. \tag{22}$$

We have combined the Faraday and geometric rotations that occur along a given leg since rotations about the same axis are additive. We have also used the existence of the plane of symmetry ACE to replace the rotation angles along AD (CD) with those of AB (BC). Looking at M^+ and M^- we see the polarization effects accompanying propagation along each leg: rotation due to the Faraday effect (γ), a rotation associated with the change of coordinate system (θ), and phase and amplitude shifts on reflection (M_j, $j = A, B, C,$ or D).

Close examination of M^+ and M^- reveals several symmetry relations. First, if we know one of the round trip Jones matrices, we can find the other one by 1) reversing the order of the individual operators, and 2) changing the sign of each Faraday rotation angle. These two rules have simple physical interpretations. Reversing the direction of propagation from a given point reverses the order in which the polarization-influencing elements are encountered. Since the round trip Jones matrices are written as operator-ordered products, reversing the propagation direction inverts the product ordering. The change of sign of the Faraday rotations is the expression (in our coordinate system convention) of the nonreciprocity of the Faraday effect.

Let us introduce some additional notation for convenience. Define the following sums (σ) and differences (δ) of geometric (θ) and Faraday (γ) angles on legs AB and BC:

$$\delta_{AB} = \theta_{AB} - \gamma_{AB}, \tag{23a}$$

$$\sigma_{AB} = \theta_{AB} + \gamma_{AB}, \tag{23b}$$

$$\delta_{BC} = \theta_{BC} - \gamma_{BC}, \tag{24a}$$

$$\sigma_{BC} = \theta_{BC} + \gamma_{BC}. \tag{24b}$$

We can rewrite M^+ and M^-, making use of (23) and (24) and noting that $M_D = M_B$ by symmetry, as

$$M^+ = M_A R(\delta_{AB})\, M_B R(-\sigma_{BC})\, M_C R(\sigma_{BC}) \cdot M_B R(-\delta_{AB}), \tag{25}$$

$$M^- = R(-\sigma_{AB})\, M_B R(\delta_{BC})\, M_C R(-\delta_{BC}) \cdot M_B R(\sigma_{AB}) M_A. \tag{26}$$

In terms of the new angles, conversion of M^+ to M^- (and vice versa) requires inversion of the product ordering and letting $\delta \rightarrow \sigma$ and $\sigma \rightarrow \delta$.

F. Eigenvalues

The eigenvalues of the round trip Jones matrices are of primary interest to us. (Recall that the eigenvalue equation for a matrix M is $ME = \lambda E$ where λ is an eigenvalue, and E is an eigenvector.) From the eigenvalues we find the losses and frequency splittings of the polarization eigenmodes of the resonator. Since M^+ and M^- are of rank two, each matrix has two complex eigenvalues and two eigenvectors. The modulus of an eigenvalue represents the factor by which the amplitude of the electric field of the eigenmode is reduced after a round trip through the unpumped cavity, and the phase of the eigenvalue contains information about the round trip phase shift of the field.

We find the two eigenvalues for a given round trip Jones matrix M ($M = M^+$ or M^-) by solving the quadratic characteristic equation

$$\lambda^2 - \lambda \,\mathrm{Tr}\,(M) + \det\,(M) = 0 \tag{27}$$

where Tr (M) denotes the trace of the matrix and det (M) denotes the determinant. The special forms of the individual Jones matrices permit us to make some analytical statements about the coefficients in the characteristic equations. Recall that all of the individual Jones matrices except for the output coupler matrix M_A are in the special unitary group SU_2. Consequently, the two round trip Jones matrix products can be written as

$$M^+ = M_A U^+, \tag{28}$$

$$M^- = U^- M_A \tag{29}$$

where U^+, $U^- \in SU_2$, and

$$U^+ = R(\delta_{AB})\, M_B R(-\sigma_{BC})\, M_C R(\sigma_{BC})\, M_B R(-\delta_{AB}), \tag{30}$$

$$U^- = R(-\sigma_{AB})\, M_B R(\delta_{BC})\, M_C R(-\delta_{BC})\, M_B R(\sigma_{AB}). \tag{31}$$

The determinant of a product is the product of the determinants, so

$$\det\,(M^+) = \det\,(M^-) = \det\,(M_A) = r_p r_s. \tag{32}$$

We note that the determinant is a positive real number $0 \le r_p r_s \le 1$. The only complex coefficients in the characteristic equations are the traces of the round trip matrices. Since the determinants of M^+ and M^- are the same, the characteristic equations and thus the eigenvalues for CCW and CW propagation differ only if Tr (M^+) $\neq$ Tr (M^-).

The sum of the two roots of (27) equals the trace of M, and the product of the two roots equals the determinant of M. These two rules have important physical consequences, as we shall see in part 2) of this section.

1) Round Trip Losses: There are four eigenvalues for the resonator, two for each of the two directions of propagation around the ring. In general, these four eigenvalues are nondegenerate and can be sorted according to their moduli. The round trip power loss of the mode with eigenvalue λ_i is

$$(\text{Loss for eigenmode i}) = 1 - |\lambda_i|^2. \tag{33}$$

The eigenmode with the lowest loss reaches laser oscillation threshold first. Since the Nd:YAG laser transition is homogeneously broadened, the first traveling-wave mode to oscillate saturates the gain uniformly and prevents the higher loss modes from reaching threshold. In this way, unidirectional, single-axial-mode operation of the ring laser is established and maintained.

In contrast stable unidirectional oscillation will not occur if the losses for CCW propagation are equal to those for CW propagation. Examination of cases in which the CCW and CW eigenvalue pairs are equal gives insight into the need for both a nonplanar ring geometry and an applied magnetic field for establishing unidirectional operation in an optically isotropic, monolithic medium. In the following two sections, we prove that stable unidirectional oscillation will not occur for either a) a planar ring with an arbitrary applied magnetic field, or b) a nonplanar ring with no applied magnetic field.

a) Planar Ring with Applied Magnetic Field: Consider an arbitrary planar ring light path in a monolithic, optically isotropic medium in an applied magnetic field. Since for a planar ring all the reflecting surfaces have coplanar normals, there are no rotations of coordinate systems about the direction of propagation to consider. The most general Jones matrix for a CCW traversal of the ring can be written in the form [37]

$$M^+ = \prod_{i=1}^{N} D_i O_i(\gamma_i) \tag{34}$$

where D_i represents a diagonal matrix (reflection matrix), and O_i represents a proper orthogonal matrix (Faraday rotation or the unit matrix). Applying the rule for obtaining M^- from M^+, we reverse the order of multiplication of the matrices and change the signs of all the Faraday rotation angles, giving

$$M^- = \prod_{i=N}^{1} O_i(-\gamma_i) D_i. \tag{35}$$

Recall that the most general proper orthogonal matrix can be written in the form of a rotation matrix. The transpose of a 2×2 rotation matrix is obtained by changing the sign of the rotation angle. Diagonal matrices are unchanged under transposition. Recalling that the transpose of a product of matrices is the product of the transposes in reverse order, we see that M^- and M^+ are transposes of one another. Since a matrix and its transpose have identical eigenvalues, there is no loss difference between the two directions of propagation, hence no preferred direction of propagation around the ring.

The nonplanar geometry circumvents this proof by introducing additional rotations whose angles do not change signs when the direction of propagation is reversed, thus making it impossible to generate the other round trip Jones matrix by transposition. In simple terms a monolithic, planar, optically isotropic medium offers no means of producing reciprocal rotation.

b) Nonplanar Ring with No Applied Magnetic Field: Next consider the case of a nonplanar ring with no applied magnetic field and hence no Faraday rotation. For concreteness let us restrict our attention to the NPRO case. Then the round trip Jones matrices are

$$M^+ = M_A R(\theta_{AB})\, M_B R(-\theta_{BC})\, M_C R(\theta_{BC}) \cdot M_B R(-\theta_{AB}), \tag{36}$$

$$M^- = R(-\theta_{AB})\, M_B R(\theta_{BC})\, M_C R(-\theta_{BC}) \cdot M_B R(\theta_{AB}) M_A. \tag{37}$$

We have already seen in (32) that the determinants of M^+ and M^- are equal. We now prove that the traces of the matrices of (36) and (37) are also equal, which implies that the CCW eigenvalues are equal to the CW eigenvalues according to (27). Recalling that cyclic permutation of matrices in a product does not change the trace of the product, we can permute the terms of M^- cyclically to get

$$\mathrm{Tr}\,(M^-) = \mathrm{Tr}\left\{M_A R(-\theta_{AB})\, M_B R(\theta_{BC})\, M_C R(-\theta_{BC}) \cdot M_B R(\theta_{AB})\right\}. \tag{38}$$

The rotation matrix $R(\alpha)$ is related to the rotation matrix $R(-\alpha)$ by the following transformation

$$R(-\alpha) = TR(\alpha)T \tag{39}$$

where T is the reflection operator

$$T = \begin{bmatrix} -1 & 0 \\ 0 & 1 \end{bmatrix}. \tag{40}$$

By inspection we can then write

$$\mathrm{Tr}\,(M^-) = \mathrm{Tr}\left\{M_A TR(\theta_{AB})T\, M_B TR(-\theta_{BC})T \cdot M_C TR(\theta_{BC})T\, M_B TR(-\theta_{AB})T\right\}. \tag{41}$$

Another cyclic permutation and use of the associativity of matrix products gives us

$$\mathrm{Tr}\,(M^-) = \mathrm{Tr}\left\{[TM_A T]\, R(\theta_{AB})[TM_B T] \cdot R(-\theta_{BC})[TM_C T]\, R(\theta_{BC})[TM_B T] \cdot R(-\theta_{AB})\right\}. \tag{42}$$

For a diagonal matrix D we have $TDT = D$, so (42) reduces to

$$\mathrm{Tr}\,(M^-) = \mathrm{Tr}\left\{M_A R(\theta_{AB})\, M_B R(-\theta_{BC})\, M_C R(\theta_{BC}) \cdot M_B R(-\theta_{AB})\right\} = \mathrm{Tr}\,(M^+). \tag{43}$$

The round trip matrices (36) and (37) for a nonplanar ring with no applied magnetic field thus have identical traces and determinants, hence by (27) they also have identical eigenvalues. We conclude that, in the absence of an applied magnetic field, the nonplanar ring geometry alone cannot produce stable unidirectional operation. The absence of the Faraday rotation makes the entire system reciprocal, so there can be no loss difference between the two directions of propagation.

The two degenerate cases described above can be explained intuitively. An optical diode requires reciprocal rotation, nonreciprocal rotation, and a polarizer. An optically isotropic monolithic medium has no reciprocal rotation if it is planar and has no nonreciprocal rotation if there is no applied magnetic field. Thus, to establish an optical diode in an NPRO we require both a nonplanar ring geometry and an applied magnetic field.

2) Frequency Splitting: So far we have considered only the losses of the eigenpolarization modes of the NPRO resonator. Equally important for our purposes are the eigenfrequencies, which are related to the round trip phase shifts. Since we eliminated isotropic phase shifts and retained only anisotropies in writing the Jones matrices, the phases of the eigenvalues explicitly yield the frequency differences among the eigenmodes.

If the resonator is isotropic, the four eigenfrequencies are identical because each eigenmode has the same optical path length around the ring. Phase anisotropy lifts this degeneracy. Recall that the product of the two eigenvalues for one direction of propagation must equal the determinant of the round trip Jones matrix. From (32) we know that the determinant is a real number. Let λ_1 and λ_2 be the two eigenvalues for, say, CCW propagation. Since the product $\lambda_1\lambda_2$ is real and since the eigenfrequencies are degenerate for the case of an isotropic resonator, the phases of λ_1 and λ_2 must be equal in magnitude and opposite in sign. Physically, the consequence is that phase anisotropy in the resonator causes the two eigenfrequencies for one direction of propagation to lie equally spaced above and below the degenerate frequency corresponding to an isotropic resonator.

We now consider all four eigenvalues. The frequency shift $\Delta\nu_i$ of the ith eigenmode away from the initially fourfold degenerate resonant frequency is

$$\Delta\nu_i = (c/nL)(\phi_i/2\pi) \tag{44}$$

where $\phi_i = \arg(\lambda_i)$ in radians, c is the speed of light, L is the round trip path length of the ring, and n is the average index of refraction of the ring path. From a pair associated with a given direction of propagation, one frequency is shifted upward and the other downward by an equal amount. The magnitudes of the shifts for the two directions of propagation are in general different.

A general NPRO resonator has four possible eigenfrequencies for its four eigenpolarizations. The existence of four different frequencies in a nonplanar ring resonator has been explored in connection with multioscillator ring laser gyroscopes (MRLG) [20] based on the He-Ne laser (see Appendix A). The MRLG resonators are painstakingly engineered to ensure that the four eigenpolarizations are circular and that all four modes oscillate simultaneously, which is possible because of the inhomogeneous broadening of the gas laser transitions. With such a spectrum of oscillating modes, it is possible to arrange that two oppositely biased ring laser gyros coexist and share the same optical path. Taking the difference between the outputs of the two coresident ring laser gyros permits the cancellation of the bias and doubles the scale factor for the gyroscope.

In the homogeneously broadened gain medium of the NPRO, only the lowest loss mode oscillates. Still, that the four possible eigenfrequencies of an NPRO are generally distinct has some important consequences for optical feedback effects. Consider the mode with the largest modulus eigenvalue. This mode oscillates first, as we explained previously. Imagine that this mode propagates in the CCW direction and that there is some backscatter in the resonator or some extracavity optical feedback. Not only does the mode with the largest CW eigenvalue suffer more loss than the oscillating CCW mode, there is generally a frequency shift between them as well. Thus, light from the oscillating CCW mode couples weakly into its closest CW competitor. Unidirectional oscillation established on the basis of differential loss between the modes gains additional stability due to the frequency splitting between the counterpropagating modes.

G. Eigenvectors

With each eigenvalue is associated an eigenvector. The eigenvector is the Jones vector of the light at the point A^+ (see Fig. 5). The eigenvector changes as it propagates through the resonator, but it reproduces itself (modulo an overall amplitude reduction and phase shift) after a round trip. If we specify the state of polarization by χ as in (3), then we find χ directly in terms of the elements of the round trip Jones matrix as [38]

$$\chi_{1,2} = \frac{M_{22} - M_{11} \pm \sqrt{\mathrm{Tr}(M)^2 - 4 \det(M)}}{2M_{12}}. \quad (45)$$

In general, the two eigenvectors for a given direction of propagation are nonorthogonal, elliptical states of polarization with different round trip losses. The nonorthogonality and loss difference are caused by the amplitude anisotropy ($\rho \neq 1$) of the partial polarizer. A resonator with no amplitude anisotropy can be represented by a special unitary round trip Jones matrix once the isotropic amplitude reduction is factored out. Such a resonator has orthogonal elliptical eigenstates with identical losses.

Special design efforts are required to produce specific eigenpolarizations in an NPRO resonator. We will solve an important special case in Section IV and show that it is possible to find linearly polarized eigenstates even in the presence of the polarization rotations in the cavity. Another special case yielding circular eigenpolarizations is described in Appendix A in connection with the multioscillator ring laser gyros.

H. Specification and Evaluation of the NPRO

Within the assumptions of our model a complete specification of an NPRO resonator requires the following information: 1) the index of refraction n and the Verdet constant V of the gain medium at the wavelength of the laser transition, 2) the uniform magnetic field $\boldsymbol{B}$ applied to the gain medium parallel to AE, 3) the moduli r_s and r_p and the relative phase shift Δ of the Fresnel amplitude reflection coefficients of the output coupler, and 4) the parameters that specify the geometry of the resonator $\{AE, CE, \theta_A, \text{and } \beta\}$.

Using the formalism developed so far we can simply choose a set of parameters for a proposed NPRO resonator, calculate the eigenvalues, and deduce the output coupling losses of the four possible eigenmodes. In general, the four losses will be different. For each direction of propagation there is a high loss mode and a low loss mode. To evaluate an NPRO design we focus our attention on the lower loss mode for each direction of propagation. The lowest loss mode is the one that will oscillate, and the threshold of the resonator can be calculated in terms of the loss of the lowest loss mode. The strength of the intracavity optical diode is equal to the difference between the losses of the two lowest loss modes (one for CCW operation, one for CW operation). We refer to this important quantity simply as the loss difference of the resonator. The two most important quantities for evaluating an NPRO design are the loss of the lowest loss mode, which determines threshold requirements and slope efficiency [10], and the loss difference of the resonator.

III. Simplified Analysis of the NPRO Resonator

The algebraic complexity of the round trip Jones matrices of (21) and (22) makes it difficult to use intuition in the design of monolithic nonplanar ring oscillators. Since there are so many parameters required to specify the resonator, we need to have some guiding principles for our design efforts. Fortunately, we can use an optical equivalence theorem of Hurwitz and Jones [22] to reduce the resonator theory to a simpler equivalent form. In this section, we introduce the optical equivalence theorem and use it to simplify the interpretation of the round trip Jones matrices for the NPRO.

A. Optical Equivalence Theorem

The optical equivalence theorem of interest to us here involves analysis of lossless polarization-influencing systems. We have seen in Section II-D that such a system is represented by a special unitary Jones matrix. Mathematically, any matrix $V \in SU_2$ can be written as a product of two rotation matrices and a diagonal element of SU_2,

$$V = R(\alpha)\, G(\psi)\, R(\beta) \tag{46}$$

where $R(\alpha)$ and $R(\beta)$ are rotation matrices as in (15), and the diagonal matrix $G(\psi)$ has the form

$$G(\psi) = \begin{bmatrix} e^{i\psi} & 0 \\ 0 & e^{-i\psi} \end{bmatrix}. \tag{47}$$

As explained by Hurwitz and Jones, this theorem has an optical interpretation: a system containing any number of linear retarders (waveplates) and rotators (any devices whose Cartesian Jones matrices are rotation matrices) can be represented by a special unitary Jones matrix and thus is equivalent to a system containing just one linear retarder (with retardance 2ψ and orientation angle α) and one rotator (with rotation angle $\alpha + \beta$). The constructive proof of the theorem given by Hurwitz and Jones explicitly gives the parameters α, β, and ψ in terms of the matrix elements of V [22].

B. Application of Optical Equivalence Theorem to NPRO

We have seen in (28) and (29) that the round trip Jones matrix M^+ (M^-) is a product of a special unitary matrix U^+ (U^-) and the nonunitary matrix M_A. The special unitary product U^+ and U^- represent the complicated net effects of all the TIR phase shifts and Faraday rotations. The optical equivalence theorem applied to U^+ and U^- yields important insight into the polarization properties of the NPRO resonator. In Appendix C we give analytical expressions for the matrix elements of U^+ and U^-, and we explicitly solve for the rotation angles α and β and the retardance parameter ψ that appear in (46). We find that $\alpha = -\beta$ in each case, so we can write

$$U^+ = R(\alpha^+)\, G(\psi^+)\, R(-\alpha^+) \tag{48}$$

$$U^- = R(\alpha^-)\, G(\psi^-)\, R(-\alpha^-). \tag{49}$$

We can therefore interpret U^+ (U^-) simply: the system represented by the Jones matrix U^+ (U^-) is optically equivalent to a single waveplate with retardance $2\psi^+$ ($2\psi^-$) whose principal axes subtend an angle α^+ (α^-) with respect to the principal axes of the output coupler; no additional rotator appears in the optically equivalent system. This important result enables us to form a simple mental picture of how the NPRO resonator affects polarization. Instead of trying to imagine how the Faraday rotations, geometric rotations, and TIR phase shifts separately influence the polarization of the intracavity radiation, we envision two different resonators. For a given direction of propagation around the ring, the NPRO resonator is optically equivalent to a waveplate and the output coupler. The principal axes of the waveplate are in general rotated with respect to those of the output coupler. The output coupler is itself optically equivalent to a half-wave plate and a partial polarizer.

The nonreciprocal effects of Faraday rotation manifest themselves as differences between the retardances $2\psi^+$ and $2\psi^-$ and orientation angles α^+ and α^- of the effective CCW and CW waveplates. We discuss these effects further in Appendix C, and we will show examples in Table I of Section IV-E.

IV. A Special Class of NPRO's with Low Threshold and Large Loss Difference

With the formalism of Section II and the optical equivalence model of Section III in mind we now address the question of how to design an NPRO resonator. Many considerations enter into the design, including resistance to optical feedback, sensitivity to environmental effects, magnetic field requirements for unidirectional operation,[3] threshold and slope efficiency, output beam quality and polarization, and frequency tunability.

We have been motivated by our goal of achieving narrow linewidth operation to consider small, low threshold NPRO's with good resistance to optical feedback. The low threshold design enables us to use low power single stripe diode lasers to end-pump the NPRO's [10], and good resistance to optical feedback is important for isolating the NPRO from frequency perturbations caused by retroreflected radiation. Arguing that output radiation reflected back into the resonator can be treated as an external signal injected into a regenerative amplifier [39], we have concluded that increasing the loss difference between the two directions of propagation is important in reducing the sensitivity to optical feedback [40].

We are thus led to consider a special class of NPRO's that simultaneously have low output coupling and a large loss difference. Trutna *et al.* [10] have previously discussed the problem of designing such an NPRO in Nd:YAG; however, they neglected the effects of Faraday rotation on legs *BC* and *CD*. In this section, we present a general strategy for finding NPRO's with low output coupling and a large loss difference in any gain medium with refractive index n and Verdet constant V. For a given applied magnetic field $\boldsymbol{B}$ parallel to *AE* our task is to choose the geometry of the resonator (specified by θ_A, *CE*, *AE*, and β) and the parameters of the output coupler (specified by r_p and r_s, or by r_s and $\rho = r_p/r_s$) to produce a low threshold NPRO with a large loss difference.

A. Rotator and Partial Polarizer

In Section III we proved that for each direction of propagation the NPRO resonator is optically equivalent to a

[3]The loss difference required to overcome internal coupling between the two directions of propagation and thereby establish unidirectional operation in a discrete-element ring has been estimated to be 0.01 percent [13]. In monolithic NPRO's a smaller loss difference should suffice since the internal coupling is reduced.

ring comprising a waveplate rotated with respect to the output coupler, which is itself modeled as an aligned combination of a half-wave plate and a linear partial polarizer. The retardances and orientation angles of the equivalent CCW and CW waveplates are coupled together in a complicated way by the constraints of the monolithic nonplanar geometry and by the amount of Faraday rotation available in typical media (see Appendix C). A rigorous discussion with all of the constraints included is complicated, so to gain some insight into how to design an NPRO with low threshold and large loss difference, imagine that we could freely choose the retardances and orientation angles of the equivalent optical systems for the two directions of propagation. Let us assume that we want the NPRO to run unidirectionally in the CCW direction. We want to have linear, s-polarized light as an eigenstate at the output coupler for CCW propagation, because that assures us of having the lowest output coupling, $1 - r_s^2$, for the given reflector. We achieve this result by forcing the optically equivalent waveplate for CCW propagation to have its principal axes aligned ($\alpha^+ = 0$) with those of the output coupler, regardless of the actual retardance $2\psi^+$ of the waveplate.

Next we want to choose the retardance and orientation angle of the CW waveplate to maximize the loss difference. Here we make one concession to the coupling of the two directions of propagation by noting that the choice $\alpha^+ = 0$ implies, for resonators with total Faraday rotation Γ, that α^- cannot exceed Γ (see Appendix C). Our analysis of this problem shows that for a given orientation angle α^- and partial polarizer, the loss difference is maximized by choosing the retardance $2\psi^-$ of the CW waveplate to be 180°, i.e., we should choose the CW waveplate to be a half-wave plate. Recall that two half-wave plates with an angle α^- between their fast axes are optically equivalent to a rotator with Jones matrix $R(2\alpha^-)$. Therefore, with $\alpha^+ = 0$ and a given orientation angle α^-, the loss difference of the resonator is maximized by arranging the CW system to be optically equivalent to a ring containing a rotator with rotation angle $2\alpha^-$ and a partial polarizer.

The properties of a ring composed of a rotator and a partial polarizer are well known [19], [41] and we review them in Appendix D. The most important point to make here is that for a given rotation angle, there is a best choice for the partial polarizer in order to maximize the loss difference. Note that the choice of the partial polarizer strength ρ of the output coupler is independent of the problem of choosing an appropriate geometry for the resonator, and the choice of r_s is dictated by the desired values for threshold and slope efficiency.

Our analysis of the rings in which we are free to choose the waveplates and orientation angles independently for the two directions of propagation motivates the following strategy for designing an NPRO resonator with a low threshold and a large loss difference. For a given medium in a given magnetic field 1) identify the subset of all possible NPRO geometries leading to aligned CCW waveplate equivalents ($\alpha^+ = 0$) to establish the minimal output coupling eigenstate, 2) within this subset search for geometries having half-wave plate equivalents ($2\psi^- = 180°$) for the CW waveplate, 3) within the subset with $\alpha^+ = 0$ and $2\psi^- = 180°$ identify the acceptable systems having the largest orientation angle α^- for the CW half-wave plate, 4) choose the partial polarizer for the system found in 3) in order to maximize the loss difference. To satisfy all of these requirements imposes many restrictions on the possible media and NPRO geometries, as we shall see.

B. CCW Waveplate Aligned with Output Coupler; CW Waveplate a Rotated Half-Wave Plate

Equations for the equivalent retardances and principal axis orientation angles of the CCW and CW unitary products U^+ and U^- are derived in Appendix C. We want the CCW unitary product to be optically equivalent to a waveplate with its principal axes aligned with those of the output coupler, and we want the CW unitary product to be optically equivalent to a half-wave plate, so we substitute $\alpha^+ = 0$ into (C.16) and (C.17) and $2\psi^- = 180°$ into (C.18–C.20). We arrive at the following two constraint equations:

$$0 = \cos(\Delta_B)\cos(\Delta_C/2) - \sin(\Delta_B)\sin(\Delta_C/2)\cos(2\delta_{BC}) \tag{50}$$

$$0 = \left[\sin(\Delta_B)\cos(\Delta_C/2) + \cos(\Delta_B)\sin(\Delta_C/2)\cdot\cos(2\sigma_{BC})\right]\sin(2\delta_{AB}) - \left[\sin(\Delta_C/2)\sin(2\sigma_{BC})\right]\cos(2\delta_{AB}). \tag{51}$$

From (50) we begin to find constraints imposed on the resonator. We can rewrite (50) as

$$\tan(\Delta_B)\tan(\Delta_C/2) = \frac{1}{\cos(2\delta_{BC})}. \tag{52}$$

Note that the right-hand side is greater than one for nonzero δ_{BC}. We have no solution unless the left-hand side is also greater than one, which puts a restriction on the phase shifts due to TIR. There is an additional constraint imposed by the geometry. We choose θ_A, AE, CE, and β. Having done so fixes θ_B and θ_C. The index of refraction n and the angles of incidence θ_B and θ_C determine the phase shifts Δ_B and Δ_C as in (14). With these rules one can show that the requirement that the left-hand side of (52) exceed one is

$$2\Delta_B + \Delta_C > 180. \tag{53}$$

This rule has an important consequence for the choice of the gain medium. In Appendix E we prove that (53) [and thus (52)] has no solution unless the index of refraction of the gain medium is greater than $\sqrt{3}$. Therefore, for media such as Nd:YAG ($n = 1.82$) and Nd:GGG ($n = 1.945$) we can find the desired NPRO geometries. For media such as Nd:glass ($n \approx 1.5$) different approaches are required, such as changing the geometry and increas-

ing the number of total internal reflection bounces to five. We will discuss these more general designs in a future publication. For now we restrict ourselves to three TIR bounces and one reflection from the output coupler per round trip.

So far we have seen that the gain medium must have a sufficiently large index of refraction if we are to find the desired NPRO geometry. The remainder of the problem consists of finding geometries that satisfy the constraints (50) and (51). Let us count the available degrees of freedom at this point. We require four parameters to specify the geometry of the resonator, and we only have two constraint equations. We therefore must choose two parameters and solve for the remaining two. We choose a value of the length AE and an angle of incidence θ_A at the output coupler, then solve the constraint equations to find the length CE and the dihedral angle β. Since the Verdet constant V and the applied magnetic field are already specified, the choice of AE pins down the amount of Faraday rotation γ_{AB} on the legs AB and AD. (Note that what really matters here is the product $VB(AE)$, so for a given Verdet constant V we can trade length for magnetic field in the product $B(AE)$.) With AE and θ_A given, we have full knowledge of the isosceles triangle ABD. We therefore search for the family of isosceles triangles BCD that lead to solutions of the constraint equations. These solutions are best found by numerically solving the transcendental constraints (50) and (51).

In the course of characterizing solutions, we have found some limitations on the possible ranges of the angles of the resonator. For example, the smallest angle of incidence on the output coupler that still leads to solutions in Nd:YAG is roughly 28.15°. This result is important because one might be inclined to try to reduce the astigmatism of the resonator by reducing θ_A, but the constraints impose a lower limit on θ_A. Formally, we can continue to find solutions for values of the angle of incidence exceeding the critical angle, but these solutions are not of interest to us since we do not want total internal reflection at the output coupler. For Nd:YAG, then, the range of acceptance θ_A is approximately 28.15–33.33°. Other materials would similarly have limited ranges of acceptable θ_A.

C. Choice of Partial Polarizer

Once we know how to solve for the geometry of the resonator for a given magnetic field and a given index of refraction and Verdet constant of the gain medium, we still need to know how to choose the output coupler. We have restricted ourselves to consideration of output couplers that act in reflection like a combination of a partial polarizer and a half-wave plate, so the problem reduces to choosing the parameters r_s and ρ of the partial polarizer.

The choice of r_s is dictated by the considerations of threshold and slope efficiency. The problem at hand is to choose the partial polarizer strength ρ so that the loss difference between the two directions of propagation is made as large as possible. Given the value of the CW equivalent rotation angle $2\alpha^-$, we want to choose the partial polarizer to give the largest possible loss difference. This problem has been solved by Kruzhalov and Kozhevnikov [41], and we derive the solution in Appendix D. For small rotation angles ($2\alpha^- << 1$ radian), the largest loss difference is obtained by choosing the partial polarizer such that $\rho = 1 - 4\alpha^-$, and the resulting loss difference is $4r_s^2\alpha^-$, with α^- in radians.

As a practical matter one cannot choose arbitrary values of the partial polarizer parameter ρ because the partial polarizer is the multilayer dielectric mirror used at oblique incidence. For quarter-wave stack designs involving high index/low index layer pairs we find that r_s and ρ both rise as the number of layer pairs is increased. Thus, the requirement of high reflectivity means that the output coupler acts as a weak partial polarizer. If the available rotation angle $2\alpha^-$ becomes large, the value of ρ consistent with having reasonable reflectivity for the s component will generally be larger than the value that maximizes the loss difference. We discuss a practical example in the following section.

D. An Example of NPRO Design for Nd:YAG

In this section, we work through an example of designing an NPRO that simultaneously offers low output coupling and a large loss difference. To make the discussion concrete, we restrict our attention to Nd:YAG as the gain medium, with $n = 1.82$ and $V = 103°\ \mathrm{T}^{-1}\ \mathrm{m}^{-1}$ at 1.06 μm. We assume a magnetic field $B = 0.5$ T in order that the desired field can be obtained by a suitable arrangement of small permanent magnets. In the interest of small size and low threshold operation, we take the characteristic length $AE = 4.0$ mm. We choose the angle of incidence at the output coupler to be $\theta_A = 30.00°$, a value in the center of the acceptable range. These values of AE and θ_A are close to those chosen by Trutna *et al.* [10], which makes possible a direct comparison of the designs.

Numerically solving the constraints (50) and (51) gives us two choices for the resonator geometry: 1) $\beta = 1.4329°$ and $CE = 1.553$ mm, or 2) $\beta = 1.0489°$ and $CE = 2.333$ mm. Both choices ultimately lead to loss differences in excess of 3.3 percent, but the solution with the smaller β yields the larger loss difference. We therefore choose the one with $\beta = 1.0489°$ and $CE = 2.333$ mm and find that $\alpha^- = 0.5409°$, and $2\psi^+ = 179.9857°$. It is interesting to compare the magnitude of α^- to the total Faraday rotation angle $\Gamma = 2(\gamma_{AB} + \gamma_{BC}) = 0.6531°$. We find that, in this example, approximately 82.8 percent of the total Faraday rotation appears as the difference between the magnitudes of the orientation angles of the CCW and CW equivalent waveplates (see Appendix C).

The next problem is finding the best value of the partial polarizer strength ρ. Using the results of Appendix D we find the optimal choice of $\rho = 0.96294$. All that remains in principle is to choose a target value for the threshold of the resonator under diode-laser end-pumping, and then to select r_s to satisfy the threshold condition. The exact value of r_s is not crucial, so let us choose r_s to give a

TABLE I

CALCULATED OPTICAL EQUIVALENTS OF THE FARADAY ROTATIONS AND TOTAL REFLECTIONS OF ALL PUBLISHED NPRO DESIGNS AND ONE OF OUR RECENT DESIGNS. FOR CCW (CW) PROPAGATION THE COLLECTIVE EFFECT OF ALL THE FARADAY ROTATIONS AND TOTAL INTERNAL REFLECTIONS IS OPTICALLY EQUIVALENT TO A WAVEPLATE WITH RETARDATION $2\psi^+$ ($2\psi^-$) WHOSE PRINCIPAL AXES ARE ROTATED BY AN ANGLE α^+ (α^-) WITH RESPECT TO THOSE OF THE OUTPUT COUPLER. THE DIHEDRAL ANGLE β CHARACTERIZING THE NONPLANARITY OF THE RING IS SHOWN FOR EACH DESIGN. THE LOSS DIFFERENCES SHOWN IN THE LAST COLUMN CANNOT BE COMPARED DIRECTLY BECAUSE LOSS DIFFERENCES DEPEND ON THE CHOICE OF THE OUTPUT COUPLING MIRROR, BUT THE LOSS DIFFERENCES ARE INDICATIVE OF THE RESULTS OBTAINED WITH VARIOUS RESONATOR DESIGNS

Calculated Parameters of Optical Equivalents of NPRO Designs					
NPRO	α^+ (degree)	$2\psi^+$ (degree)	α^- (degree)	$2\psi^-$ (degree)	Loss Difference (%)
Kane and Byer[a] $\beta = 90.000°$	15.208	96.565	−22.737	96.565	0.02
Kane *et al.*[b] $\beta = 90.000°$	22.181	78.231	−24.346	78.231	0.01
Trutna *et al.*[c] $\beta = 1.250°$	0.002	180.984	−0.451	180.994	0.60
This work[d] $\beta = 1.049°$	0.000	179.986	−0.541	180.000	3.70

[a][5]—NPRO parameter set: $\beta = 90.00°$, $\theta_A = 7.80°$, $AE = 36.50$ mm, $CE = 1.80$ mm. Mirror parameters $r_p = 0.99398$, $r_s = 0.99599$, $B = 1.00$ T.

[b][9]—NPRO parameter set: $\beta = 90.00°$, $\theta_A = 15.95°$, $AE = 10.50$ mm, $CE = 1.50$ mm. Mirror parameters $r_p = 0.98995$, $r_s = 0.99599$. $B = 1.00$ T.

[c][10]—NPRO parameter set: $\beta = 1.25°$, $\theta_A = 30.00°$, $AE = 4.23$ mm, $CE = 1.77$ mm. Mirror parameters $r_p = 0.92195$, $r_s = 0.99950$. $B = 0.43$ T. Note that the design of Trutna *et al.* was not chosen to maximize the loss difference. Fig. 3(b) of their paper shows a calculated loss difference exceeding 6 percent for a design with an applied magnetic field of 0.9 T and a dihedral angle of approximately 5°.

[d]NPRO parameter set: $\beta = 1.049°$, $\theta_A = 30.00°$, $AE = 4.00$ mm, $CE = 2.33$ mm. Mirror parameters $r_p = 0.96198$, $r_s = 0.99900$ (optimal mirror parameters). $B = 0.50$ T.

power reflection coefficient of order 99.8 percent. Can we find a standard quarter-wave dielectric stack to give us such an output coupler? If we consider stacks formed of alternating quarter-wave optical thickness layers of TiO_2 ($n = 2.251$) and SiO_2 ($n = 1.435$), we find that the stack design YAG[HL]^7 Air results in a mirror with partial polarizer strength $\rho = 0.9683$ and a power reflection coefficient for the s component of 99.87 percent. For the remainder of the paper we will continue to use the optimal value of partial polarizer strength for our calculations.

E. Comparison of Several NPRO Designs

We have proposed a specific algorithm for finding NPRO's with small output coupling and a large loss difference. Let us see how our example of Section D compares with previously published designs for Nd:YAG NPROs. In Table I we present the numerically calculated optical equivalents of all currently published NPRO designs, together with the design presented in Section D. Results are quoted to several decimal places in order to facilitate comparison with future calculations, despite the impracticality of implementing such precision in an actual device. The table shows the retardances $2\psi^+$ and $2\psi^-$ of the equivalent CCW and CW waveplates together with the orientation angles α^+ and α^- of the principal axes of the waveplates with respect to the principal axes of the output coupler. For each design we have given a complete specification of the parameters required to calculate the results shown in Table I.

The nonplanar geometry originally used by Kane and Byer [5] had a dihedral angle β of 90°. Such a large dihedral angle leads to a resonator with a small loss difference. The loss difference in such a resonator increases monotonically with increasing applied magnetic field between 0 and 1 T. In Table I we have calculated the loss differences from the two designs with $\beta = 90°$ assuming an applied field of 1.0 T, even though such a field is difficult to obtain with simple permanent magnets. Table I shows that the NPRO's with a dihedral angle of 90° have optical equivalents that are far from the desired half-wave plate solutions discussed above, as Trutna *et al.* [10] have also noted.

The design of Trutna *et al.* is closer to the desired solution. Our analysis of their resonator shows that the equivalent CCW waveplate is aligned with the principal axes of the output coupler when the applied magnetic field is 0.43 T. The CW equivalent waveplate is rotated by approximately half a degree, and its retardance is about 181°. Ideally, one wants the minimum output coupling point to coincide with the maximum loss difference point. The design of Trutna *et al.* does not accomplish this coincidence because their design approach required a compromise between loss difference and output coupling.

Our design is shown as the last entry in the table. The equivalent CCW waveplate is exactly aligned with the principal axes of the output coupler for an applied field of 0.5 T. The equivalent CW waveplate is exactly a half-wave plate, and its axes are rotated by more than half a degree. With an optimal choice of partial polarizer parameters in the output coupler, our design shows that a loss

difference of approximately 3.7 percent is possible while simultaneously maintaining the lowest output coupling for this resonator, about 0.2 percent. We present a detailed analysis of the eigenmodes of our design below.

V. Eigenpolarizations of Special NPRO Resonators

In Section II we showed how to find the eigenvalues and eigenvectors of the round trip Jones matrices of a general NPRO resonator, and in Section IV we introduced a special kind of NPRO in which, for a given value of the applied magnetic field, the CCW resonator is equivalent to a waveplate aligned with the output coupler while the CW resonator is equivalent to a rotator and a partial polarizer. Here we examine in detail the eigenvalues and eigenpolarizations of the special Nd:YAG NPRO design of Section IV-D. This particular NPRO is designed to produce optimal results in an applied magnetic field of 0.5 T. The resonator has $\theta_A = 30.00°$, $AE = 4.00$ mm, $CE = 2.33$ mm, and $\beta = 1.049°$. The mirror has Fresnel amplitude reflection coefficients with moduli $r_p = 0.96198$ and $r_s = 0.99900$, and the mirror produces a relative phase shift of π between the p and s components of the electric field. We have calculated the loss difference, output couplings, frequency shifts, azimuths, and ellipticity angles of all four possible eigenpolarizations for this NPRO as a function of applied magnetic fields ranging from 0 to 2 T, and the results are plotted in Fig. 6(a)–(e). These results are easily interpreted in terms of the rotator/partial polarizer system analyzed in Appendix D. We approximate the behavior of the NPRO as a rotator/partial polarizer (the rotation angle depends on the direction of propagation) for both CCW and CW propagation. The approximation is valid in this case because the Faraday rotation is so small that the CCW and CW optically equivalent waveplates differ from half-waveplates by less than 0.02 percent for applied magnetic fields in the range 0–2 T. The primary manifestation of the Faraday rotation in the optically equivalent rotator/partial polarizer systems is the difference in the rotation angles associated with CCW and CW propagation.

A. Losses and Loss Difference

The loss difference between the two directions of propagation as a function of applied magnetic field for our NPRO design is shown in Fig. 6(a). The distinctive shark's fin shape of this loss difference curve is typical of such NPRO's. At $B = 0$ there is no loss difference because the resonator is reciprocal. As the field is turned up the loss difference climbs rapidly to a cusped peak at the design point for the applied magnetic field, $B = 0.5$ T. Beyond the peak, the loss difference falls rapidly and levels off.

This result and the existence of a cusp in the loss difference curve are explained by Fig. 6(b), which shows the round trip losses for all four polarization eigenmodes versus the applied magnetic field. First examine the losses of the eigenpolarizations for a given direction of propagation around the ring. There is a high-loss mode and a low-loss mode. As the magnetic field increases the losses change. For CW propagation the losses rapidly approach one another until they nearly coalesce for $B \geq 0.5$ T. The losses behave differently for CCW propagation. As the field is

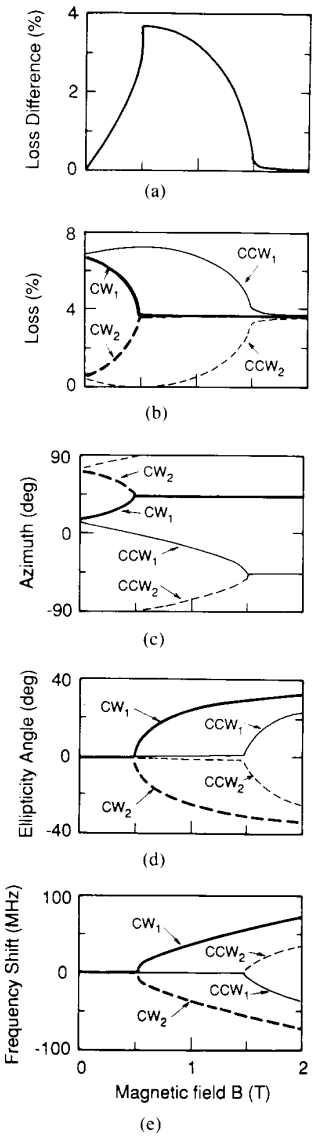

Fig. 6. Calculated magnetic field dependence of the eigenpolarization properties of a Nd:YAG NPRO resonator designed to emulate a rotator and partial polarizer. (a) Difference between the round trip losses in percent of the low-loss eigenpolarizations for CCW and CW propagation. (b) Round trip losses of the four eigenpolarizations. The low-loss eigenpolarizations are labeled CCW_2 and CW_2. The minimal loss occurs for the CCW_2 eigenpolarization at $B = 0.5$ T. (c) Azimuths of the eigenpolarizations. (d) Ellipticity angles of the eigenpolarizations. Recall that the ellipticity angle ϵ is related to the ratio of the axes of the polarization ellipse by $\tan(\epsilon) = \pm b/a$. (e) Frequency shifts of the four eigenpolarizations with respect to the initial four-fold degenerate frequency that occurs in the absence of phase anisotropy. At $B = 0$ T there is a small splitting (220 kHz, too small to see in this figure) between right-handed eigenpolarizations and left-handed eigenpolarizations. Note that the frequencies associated with a given direction of propagation split symmetrically.

increased from $B = 0$, the losses initially separate, reach a maximum separation, then rapidly approach each other, ultimately coalescing at $B \approx 1.5$ T.

The most striking feature of Fig. 6(b) is the approximate coalescence of the losses at different characteristic values of the applied magnetic field depending on the direction of propagation. Recall that for $B = 0.5$ T we rigorously forced the CW resonator to be optically equivalent to a rotator and a partial polarizer. The CCW resonator is then nearly a rotator/partial polarizer system as well, because the retardance $2\psi^+$ is nearly 180°. If we approximate the behavior of the NPRO over the entire range of magnetic field values by the rotator and partial polarizer system for both directions of propagation, then the coalescences of the losses become comprehensible. The characteristic equation of the rotator and partial polarizer system is a quadratic equation with real coefficients. As discussed in Appendix D this means that the eigenvalues for a given direction of propagation become complex conjugates for sufficiently large rotation angles. Complex conjugate eigenvalues have the same modulus, hence the corresponding eigenmodes have the same round trip loss. Moreover, the magnitude of the loss becomes independent of rotation angle above the critical point (see Appendix D). The losses for a given direction thus coalesce and clamp at a critical value of applied magnetic field.

The loss difference for the resonator at a given value of applied magnetic field [Fig. 6(a)] is the difference between the two low-loss curves of Fig. 6(b). The cusp in the loss difference curve originates from the sudden clamping of the CW loss for $B \geq 0.5$ T while the CCW loss continues to rise.

B. Eigenpolarizations

In Fig. 6(c) and (d) we show the azimuths and ellipticity angles (see Section II) of the eigenpolarizations. Recall that the azimuths are restricted to the range $-90 \leq \theta < 90°$, so the break in the curve labeled CCW_2 is only an artifact of the range restriction. The interesting behavior in both Fig. 6(c) and (d) occurs at the critical points $B = 0.5$ T and $B \approx 1.5$ T discussed in connection with the losses of the modes. We can see that the azimuths of the polarization eigenstates coalesce to $\theta \approx \pm 45°$ at the critical points. The ellipticities remain small below the critical points, then suddenly increase. The rotator and partial polarizer approximation again accounts for these effects. When the amplitude anisotropy of the partial polarizer dominates over the rotation, the resulting eigenstates are linearly polarized with azimuths that depend on the amount of rotation. When the rotation dominates over the amplitude anisotropy, the eigenstates become elliptically polarized, the azimuths remain near $\pm 45°$, and the losses become identical.

C. Frequency Splitting

Because the resonant frequencies of the polarization eigenmodes depend on the amount of Faraday rotation, the magnetic field can be used to tune the frequency of the laser, as Kane and Byer [5] noted. Fig. 6(e) shows the frequency shifts of the four polarization eigenmodes versus the applied magnetic field. On the scale of this figure there appears to be a four-fold degeneracy in the frequencies for $B = 0$ T. Actually, the reciprocal phase anisotropy of the resonator in the absence of an applied magnetic field produces a splitting between the right-handed eigenpolarizations and the left-handed eigenpolarizations. The $B = 0$ splitting for this particular resonator is only 220 kHz, so it cannot be seen in Fig. 6(e). As the magnetic field is turned on the initial two-fold degeneracies split, yielding four distinct eigenfrequencies for the four possible eigenpolarizations. For each direction of propagation we see that one eigenfrequency is upshifted while the other is downshifted by the same amount, as we explained in Section II-F.2. At $B = 0.5$ T the frequency splitting between the oscillating CCW eigenpolarization and its low-loss CW competitor is approximately 300 kHz, still not visible on the scale of Fig. 6(e). Just above $B = 0.5$ T, however, the eigenfrequencies of the pair of CW modes begin to tune rapidly. The analogous point for the CCW modes occurs at $B = 1.5$ T. Focusing attention on the low loss CCW eigenmode that will oscillate unidirectionally, we infer its tuning rate from the slope of the frequency curve. The tuning rate around the assumed bias point of 0.5 T is 240 kHz/T. Near the critical point at 1.5 T the tuning rate jumps to 12.6 MHz/T.

The sudden changes in tuning rate occur at the same critical values discussed in connection with loss coalescence. Again, the rotator and partial polarizer model explains this occurrence. For low values of magnetic field the loss anisotropy of the partial polarizer dominates over the rotation, and the resulting eigenstates are linearly polarized and frequency degenerate. (For our case this analysis is only approximate, so the eigenpolarizations are slightly elliptical, and the frequency degeneracy is lifted.) The origin of the frequency tuning is the change in effective optical path length due to the circular birefringence caused by the Faraday effect. Linearly polarized light does not experience any change in optical path length; the effect appears only for elliptically polarized light. At the critical points in the frequency splitting curves the modes in a given direction suddenly increase in ellipticity and thus experience the changing optical path length.

D. Loss Difference and the Choice of the Partial Polarizer

Fig. 7 shows how the loss difference for the NPRO resonator of Section IV-D depends on the strength of the partial polarizer. The largest loss difference for this system, 3.7 percent, occurs for a partial polarizer with $\rho = 0.96294$. The loss difference remains greater than half the peak value for partial polarizers with $0.955 \leq \rho \leq 0.980$. Note that the functional dependence of the loss difference depends on whether the polarizer is too strong ($\rho < \rho_{opt}$) or too weak ($\rho > \rho_{opt}$). When the polarizer is too weak the functional dependence is simply a straight line con-

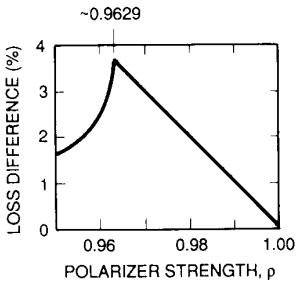

Fig. 7. The calculated loss difference of an NPRO resonator designed to emulate a rotator and partial polarizer versus the strength of the partial polarizer, defined by $\rho = r_p/r_s$. This curve is generated by holding r_s and all other resonator parameters fixed and varying only r_p. Note the sharply peaked maximum showing that the loss difference is maximized by choosing a partial polarizer with an optimal polarizing strength determined by the amount of rotation available.

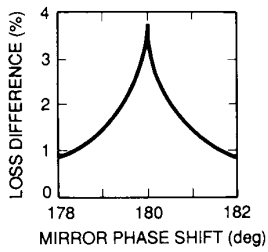

Fig. 8. The calculated loss difference of an NPRO resonator designed to emulate a rotator and partial polarizer versus the phase shift on reflection from the output coupler at A. All resonator parameters except for the phase shift on reflection from the output coupler at A are held fixed for the calculation of this curve, and the partial polarizer strength that maximizes the loss difference for a phase shift of 180° is used.

necting the maximal loss difference at $\rho = \rho_{opt}$ to the zero loss difference at $\rho = 1.0$, where there is no amplitude anisotropy.

E. Consequences of Errors in Relative Phase Shift on Reflection from the Output Coupler

Our assumption of exactly 180° relative phase shift on reflection from the output coupler is difficult to realize in practice, so it is important to understand the consequences of phase shift errors on performance. Fig. 8 shows the loss difference for the resonator as a function of the phase shift on reflection from the output coupler in the vicinity of the design point of 180°, assuming that the optimal partial polarizer strength is achieved. All of the resonator parameters except for the phase shift on reflection from the output coupler are held fixed for this calculation. The full width at half maximum of the loss difference versus phase shift curve is less than 2°, so the tolerance requirements are tight. Similar curves can be calculated for other sources of round trip phase shift error, such as imprecise knowledge of the index of refraction. We will present an analysis of the geometric, phase shift, and magnetic field tolerances of the NPRO in a future paper.

VI. Optimization Schemes

In Section IV we considered a particular form of optimization of NPRO design in which we sought to produce NPRO's that simultaneously achieve low output coupling and a large loss difference at a specific value of the applied magnetic field. The theory of Sections II and III makes possible many different optimization approaches, however, and in this section we discuss some results of alternative schemes.

Consider the general problem of attempting to choose NPRO designs to maximize some particular figure of merit. If the figure of merit is sufficiently complicated, the intuitive approaches that have proved useful to date may become difficult to apply. In that case, a natural and powerful alternative is to apply Simplex optimization to the problem [42]. The primary barrier to getting useful and believable results from the Simplex approach is the large number of parameters that enter into an NPRO design, together with the difficulty of picturing the figure of merit surface. In addition one must generally constrain the parameters to some useful region. Angles of incidence at the output coupler exceeding the critical angle frequently occur in unconstrained searches, for example.

As a specific example of applying Simplex techniques we consider the problem of maximizing the loss difference of a Nd : YAG NPRO with fixed characteristic length $AE = 4.00$ mm and angle of incidence $\theta_A = 30.00°$ in a magnetic field of 0.5 T. For simplicity we set $r_s = 0.99900$ so the NPRO is specified by the set $\{CE, \beta, \rho\}$. We have examined two types of maximization of the loss difference for such an NPRO. In the first case we fixed $\rho = 0.96294$ and allowed the Simplex to vary CE and β to find the best result. This calculation affords us a direct comparison with the approach used in Section IV-D to design the minimal output coupling/large loss difference resonator. In the second case we let the Simplex vary the partial polarizer strength ρ as well.

The result of Simplex optimization of loss difference for this NPRO resonator is essentially identical to the result of Section IV-D. In other words, the Simplex optimization arrives at the same design that our intuitive algorithm produced. We conclude that, at least for this example, the loss difference produced by our intuitive algorithm and the optimally chosen partial polarizer is the largest loss difference available for such an NPRO.

The result of allowing the Simplex to vary ρ as well is quite different. In this case, the loss difference surface has local minima in it, which makes it difficult to decide when the best result has been achieved. For the case at hand, we have found that the geometry that leads to a maximal loss difference differs dramatically from previously considered designs, and the maximal loss difference is accompanied by large output coupling. The best result found by the Simplex algorithm has a loss difference of 9.357 percent and an output coupling of 6.399 percent. These results are obtained with a partial polarizer with $\rho = 0.84245$ and $r_s = 1.00$. Unfortunately, the large output coupling puts such a design out of the range of interest for laser diode pumping, and the extreme amplitude an-

isotropy of the output coupler is not compatible with highly reflecting quarter-wave stack designs.

One could clearly include more parameters in the Simplex searches as desired. We have only performed constrained optimization studies as discussed above, but we believe that our constraints are well chosen. The point we emphasize is that our theory, together with Simplex or analogous techniques, makes it possible to study and optimize the desired properties of general NPRO's.

VII. Extensions of the Theory

In Sections I–VI we have presented an eigenpolarization theory that applies to monolithic, optically isotropic resonators with four reflections arrayed in a nonplanar ring geometry. Three of the reflectors are total internal reflections, one is an oblique reflection from a standard quarter-wave multilayer stack. If we change any of these assumptions, there are new effects to consider. In this section, we outline some of the interesting possibilities for extending our formalism to new devices.

Anisotropic Media: We have only considered optically isotropic gain media thus far. A rich class of problems based on uniaxial and biaxial media remains to be explored. Several difficulties arise in connection with propagation in anisotropic media, however, including birefflection at interfaces, Poynting vector walk-off, and thermally sensitive birefringence. For the same reason, we have not modeled the effects of stress applied to initially isotropic media, although photoelastic tuning appears to be a promising approach for frequency tuning a monolithic NPRO [43]. Applied stress breaks the isotropy of the medium. We believe that planar, unidirectional rings are possible in anisotropic media. The reciprocal polarization effect required for the optical diode can be provided by the birefringence of the anisotropic medium.

Composite Cavities: One of the great advantages of the NPRO is its monolithic construction. Composite cavities introduce new interfaces, which lead to increased coupling between the two directions of propagation. Composite cavities are also less rugged than monolithic cavities. Still, there are many reasons for examining composite cavities. Among them are the possibility of making cavities with reduced thermal sensitivity by using two or more materials that compensate for each other's thermooptic behaviors, the possibility of incorporating strong Faraday rotators into the cavity, and the prospect of using an electrooptic medium in part of the cavity. If an electrooptic medium can be incorporated, then electrooptic tuning of the frequency of the laser will be possible. We are currently investigating some of these possibilities.

Exotic Mirrors: So far our theory has assumed that the four intracavity reflections are total internal reflections from three bare surfaces and one reflection from a standard quarter-wave stack mirror. The TIR phase shifts, which play a major role in our choice of optimal geometry for a given medium, can be varied by the use of coatings on the TIR surfaces. Similarly, the phase shift on reflection from the output coupler can be varied by changing the dielectric stack design. These degrees of freedom will open up a much wider class of geometries for consideration. Controlling the precise phase shifts on reflection by the manipulation of dielectric films is an expensive proposition, however, and we have not modeled the possibilities.

Our discussion of mirrors has thus far excluded magnetooptic effects. Magnetic Kerr effect mirrors offer an additional means of inducing nonreciprocal rotation, as has been explored in connection with the MRLG schemes [44]. If magnetooptic mirrors are used, the Faraday rotation requirements of the gain medium may be reduced.

Different Geometries: As we mentioned in Section IV-B there are some advantages to considering geometries with more total internal reflection bounces than the three used in the NPRO's discussed here, particularly for a monolithic gain medium with an index of refraction smaller than $\sqrt{3}$. Even for materials with a sufficiently high index of refraction, the extra phase shifts accumulated on additional total internal reflections can be used to relax some of the constraints on the allowable angles of incidence at the output coupler, for example. We will discuss these more complicated nonplanar geometries in a future publication.

VIII. Conclusion

We have presented a comprehensive theory of the eigenpolarizations of the monolithic nonplanar ring oscillator (NPRO). The explicit round trip Jones matrices derived in Section II make it possible to perform numerical evaluations of the eigenpolarizations, losses, and frequency splittings for any NPRO. The use of the optical equivalence theorem in Section III provides an intuitive understanding of the resonator. Armed with intuition and the analytical expressions, the design of NPRO's with specific properties becomes possible. In Sections IV and V we designed and numerically analyzed a type of NPRO whose inherent optical diode best emulates the ideal discrete-element format of a rotator and a partial polarizer. This resonator has linearly polarized output, low round trip loss for the oscillating mode, and a large loss difference. For such a resonator we showed that there is a best choice for the partial polarizer strength of the output coupler, leading to maximal loss nonreciprocity.

We proved analytically that stable unidirectional operation of the NPRO requires both the nonplanar ring geometry and an applied magnetic field. We also proved that NPRO's with resonators analogous to the rotator and partial polarizer model do not exist for media with an index of refraction less than $\sqrt{3}$, and we mentioned that nonplanar rings involving a larger number of total internal reflections can overcome this restriction.

We now conclude with a discussion of the prospects for further narrowing the linewidth of the NPRO. Experimentally, free-running linewidths of less than 3 kHz have been observed to date [9]. This linewidth should be compared with the Schawlow–Townes quantum limit [45], [46] of less than 1 Hz for a Nd:YAG NPRO with a round

trip path of 1 cm, round trip loss of 1 percent, and output power of 1 mW. Clearly, there is much room for improvement in making narrow linewidth NPRO's. At some point efforts to improve the passive stability of the NPRO will cease to be useful, and active locking of the NPRO frequency to an external standard will be essential. Servo loops that use the temperature of the laser crystal, the applied magnetic field, or applied stress as control variables will enable us to lock the NPRO to a passive Fabry–Perot resonator. Such an actively stabilized system should exhibit improved short-term frequency stability.

Long-term control of the frequency may be possible by locking the second harmonic of the Nd:YAG NPRO radiation to hyperfine spectral features of molecular iodine [47], or perhaps by locking the 1.06 μm fundamental directly to hyperfine spectral features of Cs_2 [48]. Looking still further into the future, it may one day be possible to lock the NPRO to a spectral feature of a single atom or ion in a trap [49]. The NPRO technology makes the possibility of a solid-state laser operating with a quantum-limited linewidth seem less a remote dream and more an area for active research.

Appendix A
Nonplanar Rings

In this Appendix we review the literature on nonplanar ring lasers and discuss how the monolithic NPRO relates to previous discrete-element nonplanar ring designs. Nonplanar rings with an even number of reflections cause reciprocal polarization rotation analogous to natural optical activity and have been most thoroughly investigated in connection with clear-path multioscillator ring laser gyroscopes (MRLG) based on the He-Ne Zeeman laser. This work has been described in recent publications [20], [50]–[52] and is related to our own. The goal of the MRLG work is rotation sensing, which requires that counterpropagating modes coexist in the resonator, whereas we want unidirectional, single-mode oscillation. Both the MRLG and the NPRO use reciprocal rotation arising from the nonplanar ring geometry and nonreciprocal rotation established by applying a longitudinal magnetic field to the gain medium to achieve the desired performances. The MRLG resonator is designed to have no amplitude anisotropy. The goal is to establish four coresident circularly polarized eigenmodes with equal losses and different frequencies. In our work, on the other hand, we design the monolithic solid-state resonator so that only one of four possible modes will oscillate. The homogeneous broadening of the Nd:YAG gain medium makes this process straightforward. We use the loss differences to force unidirectional oscillation, and the frequency differences are chosen to help reduce the effects of intracavity and extracavity optical feedback on the stability of the single oscillating mode.

To our knowledge, the earliest proposed application of nonplanar ring resonators is that of Arnaud [18], who applied the idea of image rotation to the design of optical cavities in which an arbitrary ray retraces its own path after a single round trip. The first application of nonplanar ring concepts to laser gyroscopes was reported by Jacobs [53], [54]. He used six mirrors arrayed in two planes to form an isotropic cavity for a CO_2 laser gyro. The goal was to balance out the anisotropy of three mirrors in one plane with the anisotropy of the three mirrors in the second plane. A similar concept involving the MRLG has recently been patented by Sanders and Anderson [55].

Nonplanar rings have also been investigated outside of the laser gyroscope context. In 1979, Biraben [19] suggested using the reciprocal polarization rotation of a nonplanar ring as a component of an optical diode to improve the performance of unidirectional, traveling-wave, CW dye ring lasers. The same idea is applied in the NPRO in a monolithic setting. Discrete-element Nd:YAG nonplanar rings have been investigated by Smyshlyaev *et al.* [56], Golyaev *et al.* [57]–[59], and Nanii and Shelaev [60].

A large body of theoretical work on the properties of nonplanar ring lasers has been developed. The theory of stability of the optical axis of nonplanar rings is described in references [61]–[67]. Calculations of spatial mode properties are presented in [20], [68], and [69]. Polarization theory similar to what we present here is found in [18]–[20], [51], [52].

Appendix B
Nonplanar Ring Geometry

We have chosen to specify the geometry of the nonplanar ring light path by the lengths AE and CE and the two angles θ_A and β [see Fig. 3(b)]. In this Appendix, we give the transcendental equations from which we find the angles of incidence θ_C and $\theta_B (= \theta_D)$ and the coordinate system rotation angles θ_{AB} and θ_{BC}.

First, we solve for the angle of incidence at C. Since isosceles triangles ABD and BCD share the common base BD, we have

$$\tan(\theta_C) = \frac{AE}{CE} \tan(\theta_A). \tag{B.1}$$

The reflection at C is required to be a total internal reflection bounce, so θ_C must exceed the critical angle of incidence determined by the index of refraction of the NPRO medium from the formula $\sin(\theta_{\text{critical}}) = 1/n$. For Nd:YAG with index of refraction equal to 1.82 for radiation of wavelength 1.06 μm, the critical angle is approximately 33.33°.

Once we have found θ_C, we can solve for the remaining three angles using the following equations:

$$\cos(2\theta_B) = \sin(\theta_A)\sin(\theta_C) - \cos(\theta_A)\cos(\theta_C)\cos(\beta) \tag{B.2}$$

$$\cos(\theta_{AB}) = \frac{\sin(\theta_C)\cos(\theta_A) + \cos(\theta_C)\sin(\theta_A)\cos(\beta)}{\sin(2\theta_B)} \tag{B.3}$$

$$\cos(\theta_{BC}) = \frac{\sin(\theta_A)\cos(\theta_C) + \cos(\theta_A)\sin(\theta_C)\cos(\beta)}{\sin(2\theta_B)}. \quad \text{(B.4)}$$

We require total internal reflection at B and D, so $\theta_B (= \theta_D)$ must also exceed the critical angle.

Appendix C
Derivation of Matrix Elements of U^+ and U^-; Optical Equivalence Theorem

In this Appendix, we apply the optical equivalence theorem of Hurwitz and Jones to the special unitary matrices U^+ and U^- of (30) and (31). We seek expressions for the matrix elements of $U^+(U^-)$, and from these we want to solve for the rotation angles $\alpha^+(\alpha^-)$ and $\beta^+(\beta^-)$ and the retardance $2\psi^+(2\psi^-)$ of the optically equivalent system. We explicitly derive these parameters for the matrix U^+. The result for U^- is then found by the substitutions $\delta \to -\sigma$, $\sigma \to -\delta$, as can be seen by inspection of (30) and (31). Since U^+ is in SU_2 we need only evaluate U_{11}^+ and U_{21}^+. Recall the expression for U^+ from (30):

$$U^+ = R(\delta_{AB})\{M_B[R(-\sigma_{BC})M_C R(\sigma_{BC})]M_B\}R(-\delta_{AB}). \quad \text{(C.1)}$$

This product is most easily evaluated by starting in the middle at M_C. M_C undergoes an orthogonal transformation by the rotation matrix $R(\sigma_{BC})$. The resulting matrix is premultiplied and postmultiplied by the diagonal matrix M_B. Finally, this product undergoes an orthogonal transformation by the rotation matrix $R(-\delta_{AB})$. Using the explicit expressions for the individual Jones matrices given in Section II-D, we arrive at the following results for the real and imaginary parts of the matrix elements U_{11}^+ and U_{21}^+:

$$\text{Re } U_{11}^+ = \{\cos(\Delta_B)\cos(\Delta_C/2) - \sin(\Delta_B) \cdot \sin(\Delta_C/2)\cos(2\sigma_{BC})\} \quad \text{(C.2)}$$

$$\text{Im } U_{11}^+ = [\sin(\Delta_B)\cos(\Delta_C/2) + \cos(\Delta_B)\sin(\Delta_C/2) \cdot \cos(2\sigma_{BC})]\cos(2\delta_{AB}) + [\sin(\Delta_C/2)\sin(2\sigma_{BC})]\sin(2\delta_{AB}) \quad \text{(C.3)}$$

$$\text{Re } U_{21}^+ = 0 \quad \text{(C.4)}$$

$$\text{Im } U_{21}^+ = [\sin(\Delta_B)\cos(\Delta_C/2) + \cos(\Delta_B)\sin(\Delta_C/2) \cdot \cos(2\sigma_{BC})]\sin(2\delta_{AB}) - [\sin(\Delta_C/2) \cdot \sin(2\sigma_{BC})]\cos(2\delta_{AB}). \quad \text{(C.5)}$$

According to the optical equivalence theorem (46) we can write U^+ in the form

$$U^+ = R(\alpha^+)G(\psi^+)R(\beta^+). \quad \text{(C.6)}$$

Multiplying out the right-hand side of (C.6) we find

$$\text{Re } U_{11}^+ = \cos(\alpha^+ + \beta^+)\cos(\psi^+) \quad \text{(C.7)}$$

$$\text{Im } U_{11}^+ = \cos(\alpha^+ - \beta^+)\sin(\psi^+) \quad \text{(C.8)}$$

$$\text{Re } U_{21}^+ = = \sin(\alpha^+ + \beta^+)\cos(\psi^+) \quad \text{(C.9)}$$

$$\text{Im } U_{21}^+ = = \sin(\alpha^+ - \beta^+)\sin(\psi^+). \quad \text{(C.10)}$$

Equating the different expressions for the matrix elements U_{11}^+ and U_{21}^+ gives us four real equations:

$$\cos(\alpha^+ + \beta^+)\cos(\psi^+) = \{\cos(\Delta_B)\cos(\Delta_C/2) - \sin(\Delta_B) \cdot \sin(\Delta_C/2)\cos(2\sigma_{BC})\} \quad \text{(C.11)}$$

$$\cos(\alpha^+ - \beta^+)\sin(\psi^+) = [\sin(\Delta_B)\cos(\Delta_C/2) + \cos(\Delta_B)\sin(\Delta_C/2) \cdot \cos(2\sigma_{BC})]\cos(2\delta_{AB}) + [\sin(\Delta_C/2) \cdot \sin(2\sigma_{BC})]\sin(2\delta_{AB}) \quad \text{(C.12)}$$

$$\sin(\alpha^+ + \beta^+)\cos(\psi^+) = 0 \quad \text{(C.13)}$$

$$\sin(\alpha^+ - \beta^+)\sin(\psi^+) = [\sin(\Delta_B)\cos(\Delta_C/2) + \cos(\Delta_B)\sin(\Delta_C/2) \cdot \cos(2\sigma_{BC})]\sin(2\delta_{AB}) - [\sin(\Delta_C/2) \cdot \sin(2\sigma_{BC})]\cos(2\delta_{AB}). \quad \text{(C.14)}$$

From (C.11) and (C.13) we see that $\alpha^+ = -\beta^+$. Equation (C.13) reduces to an identity, and we are left with three equations:

$$\cos(\psi^+) = \{\cos(\Delta_B)\cos(\Delta_C/2) - \sin(\Delta_B) \cdot \sin(\Delta_C/2)\cos(2\sigma_{BC})\} \quad \text{(C.15)}$$

$$\cos(2\alpha^+)\sin(\psi^+) = [\sin(\Delta_B)\cos(\Delta_C/2) + \cos(\Delta_B)\sin(\Delta_C/2) \cdot \cos(2\sigma_{BC})]\cos(2\delta_{AB}) + [\sin(\Delta_C/2) \cdot \sin(2\sigma_{BC})]\sin(2\delta_{AB}) \quad \text{(C.16)}$$

$$\sin(2\alpha^+)\sin(\psi^+) = [\sin(\Delta_B)\cos(\Delta_C/2) + \cos(\Delta_B)\sin(\Delta_C/2) \cdot \cos(2\sigma_{BC})]\sin(2\delta_{AB}) - [\sin(\Delta_C/2) \cdot \sin(2\sigma_{BC})]\cos(2\delta_{AB}). \quad \text{(C.17)}$$

There is just one rotation angle and one retardance parameter required for the optical equivalent of U^+, which means that U^+ is optically equivalent to a single waveplate having retardance $2\psi^+$, with its principal axes rotated by angle α^+ with respect to the principal axes of the output coupler. No additional rotator is required.

The three equations for the optical equivalent of U^- are found directly from the equations for U^+ by the substitutions $\delta \to -\sigma$ and $\sigma \to -\delta$ in (C.15)-(C.17):

$$\cos(\psi^-) = \{\cos(\Delta_B)\cos(\Delta_C/2) - \sin(\Delta_B)\sin(\Delta_C/2)\cos(2\delta_{BC})\} \quad (C.18)$$

$$\cos(2\alpha^-)\sin(\psi^-) = [\sin(\Delta_B)\cos(\Delta_C/2) + \cos(\Delta_B)\sin(\Delta_C/2)\cdot\cos(2\delta_{BC})]\cos(2\sigma_{AB}) + [\sin(\Delta_C/2)\cdot\sin(2\delta_{BC})]\sin(2\sigma_{AB}) \quad (C.19)$$

$$\sin(2\alpha^-)\sin(\psi^-) = -[\sin(\Delta_B)\cos(\Delta_C/2) + \cos(\Delta_B)\sin(\Delta_C/2)\cdot\cos(2\delta_{BC})]\sin(2\sigma_{AB}) + [\sin(\Delta_C/2)\cdot\sin(2\delta_{BC})]\cos(2\sigma_{AB}). \quad (C.20)$$

Examination of (C.15) and (C.18) reveals that the retardances associated with the CCW and CW propagation directions do not depend on θ_{AB} or γ_{AB}, and the retardances differ only through the replacement of σ_{BC} by δ_{BC}. These results have a simple explanation. Consider the product that defines U^+, (C.1). The outermost rotation matrices involving σ_{AB} perform a similarity transformation on the product inside the brackets. The product in brackets is itself a product of retardation and rotation matrices and is optically equivalent to a similarity transformation of the Jones matrix of a single waveplate. We thus see that the retardation parameter ψ^+ is completely determined by the product in the brackets of (C.1) and does not depend on θ_{AB} or γ_{AB}. Similar comments apply to U^-, the only difference being the replacement of σ_{BC} by δ_{BC} inside the brackets because of the nonreciprocity of the Faraday effect.

Observe that $\sigma_{BC} = \delta_{BC}$ if there is no applied magnetic field or if the dihedral angle β is 90°, because then $\gamma_{BC} = 0$. When $\sigma_{BC} = \delta_{BC}$, the retardances of the equivalent waveplates for CCW and CW propagation are identical. Examples of this effect appear in Table I for the two geometries with $\beta = 90°$. For these geometries the nonreciprocity appears only in the orientation of the equivalent waveplates with respect to the principal axes of the output coupler. In general, however, the retardance parameters for CCW and CW propagation differ slightly, as the entries in Table I with $\beta \neq 90°$ show. For such resonators the nonreciprocity appears in both the retardances and the orientations of the equivalent waveplates.

For most cases of interest the angles σ and δ will be small, and we can expand (C.15)–(C.20) to first order in these angles. For the special case in which we have found geometries leading to $\alpha^+ = 0$ and $2\psi^- = \pi$, we can derive useful approximations for the differences between the retardances and orientation angles. In the following expressions, all angles are in radians:

$$(2\psi^- = \pi) \Rightarrow 2\psi^+ \approx \pi - 16\sin(\Delta_B)\sin(\Delta_C/2)\theta_{BC}\gamma_{BC} \quad (C.21)$$

$$(\alpha^+ = 0) \Rightarrow \alpha^- \approx 2(\gamma_{AB} + \sin(\Delta_C/2)\gamma_{BC}). \quad (C.22)$$

These approximate expressions reveal two important behaviors that are hard to see in the exact results. In the small angle limits, the CCW and CW retardances are nearly identical, and the difference between the magnitudes of the orientation angles is smaller than the total Faraday rotation $\Gamma = 2(\gamma_{AB} + \gamma_{BC})$. The Faraday rotation on legs *AB* and *AD* contributes fully to the orientation angle difference, but the Faraday rotation on legs *BC* and *CD* has its contribution reduced by the factor $\sin(\Delta_C/2)$.

Appendix D
Rotator and Partial Polarizer

Here we review the polarization eigenmodes of a ring resonator containing a rotator and a partial polarizer [19], [28], [41], [70]. We first derive and discuss the eigenvalues of the system. In particular, we derive the loss difference for an optical system consisting of a partial polarizer and a rotator in which the magnitude of the rotation angle depends on the direction of propagation. We assume that the CCW rotator is arranged to be a null rotator and that the CW rotator rotates the azimuth of an incident polarization state by the angle ϕ^- in the positive sense.

The round trip matrices for CCW (superscript +) and CW (supercript −) propagation are

$$M^+ = P(\rho)R(\phi^+ = 0) = P(\rho) \quad (D.1)$$

$$M^- = R(\phi^-)P(\rho) \quad (D.2)$$

where the Jones matrix $P(\rho)$ for the linear partial polarizer used here is given by

$$P(\rho) = r_s\begin{bmatrix}\rho & 0\\ 0 & 1\end{bmatrix} \quad (D.3)$$

and the Jones matrix $R(\phi)$ for a rotator is given by

$$R(\phi) = \begin{bmatrix}\cos(\phi) & -\sin(\phi)\\ \sin(\phi) & \cos(\phi)\end{bmatrix}. \quad (D.4)$$

By inspection of (D.1) we see that the eigenvectors of the CCW system containing a null rotator and a partial polarizer are simply the linear polarization states aligned with the principal axes of the partial polarizer. We represent the partial polarizer by a digonal matrix with diagonal elements $r_p(=\rho r_s)$ and r_s, and we assume that $r_s > r_p$. The larger eigenvalue for CCW propagation is thus r_s, and the round trip loss for CCW propagation is $1 - r_s^2$.

For CW propagation we find the eigenvalues of the round trip Jones matrix by solving the characteristic equation $\lambda^2 - \lambda\,\mathrm{Tr}(M^-) + \det(M^-) = 0$. The trace of the CW roundtrip Jones matrix is $r_s(1+\rho)\cos(\phi^-)$, and the determinant is $r_s^2\rho$. Note that both of these coefficients in the quadratic characteristic equation are real for this system, so we immediately know that the eigenvalues for CW propagation fall into three categories: 1) real and

nondegenerate, 2) real and degenerate, or 3) complex conjugates. Explicitly, the CW eigenvalues are given by

$$\lambda_{1,2} = \frac{r_s}{2}\left\{(1+\rho)\cos(\phi^-) \pm \sqrt{(1+\rho)^2\cos^2(\phi^-) - 4\rho}\right\} \quad \text{(D.5)}$$

where $\rho = r_p/r_s$, and $0 \le \rho \le 1$.

The eigenvalues are real and nondegenerate when the radicand is positive, real and degenerate when the radicand is zero, and complex conjugates when the radicand is negative. The eigenpolarizations associated with real eigenvalues are linearly polarized and have the same eigenfrequency. The eigenpolarizations associated with complex conjugate eigenvalues are elliptical, and they have the same loss. A further important property of the complex conjugate eigenvalues appears when we examine the square of their modulus, which is simply $r_s^2\rho$. Note that this result is independent of the rotation angle ϕ^-. Consider the behavior of the eigenvalues as the CW rotation angle ϕ^- is slowly increased from 0. At first, the CW eigenvalues are real and nondegenerate. At a critical value of rotation determined by the strength of the partial polarizer, i.e., when $\cos(\phi^-) = 2\sqrt{\rho}/(1+\rho)$, the CW eigenvalues are real and degenerate. For larger rotation angles the CW eigenvalues are complex conjugates and hence have identical moduli, and the moduli are independent of the rotation angle until the radicand of the characteristic equation again becomes nonnegative. Plots of eigenvalues for such systems are shown in [41].

To apply the above results to the problem of minimizing the CCW output coupling and then maximizing the loss difference of the NPRO resonator subject to the minimal output coupling constraint, recall that we have a fixed upper bound to the amount of polarization rotation available for the CW direction of propagation. (See Appendix C.) We want to make the larger modulus of the CW eigenvalues as small as possible by our choice of the partial polarizer strength ρ, given a fixed ϕ^-. Inspection of (D.5) reveals that the best choice of ρ is the one that makes the radicand exactly zero. Therefore, we want to choose ρ such that

$$\rho^2 + \left(2 - \frac{4}{\cos^2(\phi^-)}\right)\rho + 1 = 0. \quad \text{(D.6)}$$

The CW rotation angle ϕ^- is typically small in the problems of interest to us since it is determined by the amount of Faraday rotation available in the gain medium. We can therefore solve for ρ to first order in the small angle ϕ^-:

$$\rho = 1 \pm 2\phi^-. \quad \text{(D.7)}$$

Since we require $\rho \le 1$, the admissible solution is $\rho = 1 - 2\phi^-$. The corresponding eigenvalue is

$$\lambda = r_s(1 - \phi^-). \quad \text{(D.8)}$$

The loss difference is given by $2r_s^2\phi^-$. In the interest of low threshold operation r_s^2 is nearly one, so the loss difference available in a system that is optically equivalent to a rotator and an optimally chosen partial polarizer depends primarily on the available rotation. For our system the amount of rotation is limited by the small Faraday rotations accessible with small crystals and reasonable magnetic fields.

Appendix E
Derivation of Minimal Refractive Index Constraint

In this Appendix we prove that the minimal refractive index for which we can solve

$$\tan(\Delta_B)\tan(\Delta_C/2) = \frac{1}{\cos(2\delta_{BC})} \quad \text{(E.1)}$$

is $n_{\min} = \sqrt{3}$. The restriction arises from the existence of a maximum TIR phase shift for a given index of refraction:

$$\tan\left(\frac{\Delta_{\max}}{2}\right) = \frac{n^2 - 1}{2n}. \quad \text{(E.2)}$$

Note that the right-hand side of (E.1) is greater than one if δ_{BC} is nonzero. To have any hope of a solution, we at least require the left-hand side to exceed one. Since the tangent functions are monotonic, we can derive a cutoff value of the TIR phase shifts that might lead to solutions of (E.1) as follows. Set each of Δ_B and Δ_C equal to $\Delta_{\max}$ to make the left-hand side as large as possible. Then equate the left-hand side to one in order to find the smallest admissible index of refraction. The resulting equation is

$$\frac{2\tan^2(\Delta_{\max}/2)}{1 - \tan^2(\Delta_{\max}/2)} = 1. \quad \text{(E.3)}$$

Solving, we find $\tan(\Delta_{\max}/2) = 1/\sqrt{3}$. Plugging this result for $\tan(\Delta_{\max}/2)$ back into (E.2) enables us to solve for $n_{\min}$. The equation is

$$n_{\min}^2 - \frac{2}{\sqrt{3}}n_{\min} - 1 = 0. \quad \text{(E.4)}$$

The roots of this equation are $-1/\sqrt{3}$ and $\sqrt{3}$. The negative index of refraction is not physically permissible, which leaves us with the result $n_{\min} = \sqrt{3}$. This result can be given a more mnemonic interpretation. The minimum index of refraction required to give a cumulative TIR phase shift of 180° in three bounces is $n_{\min} = \sqrt{3}$.

We have as yet made no use of the constraints imposed by the geometry. The nonplanar ring light path requires that the inequality

$$\theta_A + 2\theta_B + \theta_C \le 180 \quad \text{(E.5)}$$

must hold, with the equality true only for the case $\beta = 0$. For $n = \sqrt{3}$ the maximum TIR phase shift in one bounce is 60° and occurs for an angle of incidence 45°. Setting $\theta_B = \theta_C = 45°$, the constraint on θ_A is $\theta_A < 45°$. In fact we can derive a relation between θ_A and β since we know

θ_B and θ_C. The relation is

$$\tan(\theta_A) = \cos(\beta) \qquad \text{(E.6)}$$

which has allowed solutions for β between 0 and 90°.

IX. Acknowledgment

We thank T. J. Kane, whose invention, early modeling work, and continued contributions made this work possible. We also acknowledge C. D. Nabors, J. Unternahrer, and E. C. Rea, Jr. for the numerous helpful discussions we have shared.

References

[1] H. Gerhardt, V. Bodecker, and H. Welling, "Frequency behavior of a frequency-stable YAG:Nd^{3+} laser," (in German), *Z. Angew. Phys.*, vol. 31, pp. 11-15, 1970.

[2] Y. L. Sun and R. L. Byer, "Submegahertz frequency-stabilized Nd:YAG oscillator," *Opt. Lett.*, vol. 7, pp. 408-410, 1982.

[3] K. C. Peng, Ling-An Wu, and H. J. Kimble, "Frequency-stabilized Nd:YAG laser with high output power," *Appl. Opt.*, vol. 24, pp. 938-940, 1985.

[4] T. J. Kane and R. L. Byer, "Solid-state nonplanar internally reflecting ring laser," U. S. Patent 4 578 793, 1986.

[5] T. J. Kane and R. L. Byer, "Monolithic, unidirectional single-mode Nd:YAG ring laser," *Opt. Lett.*, vol. 10, pp. 65-67, 1985.

[6] A. E. Siegman, *Lasers*. Mill Valley, CA: University Science Books, 1986, pp. 535-536.

[7] H. G. Danielmeyer, "Progress in Nd:YAG lasers," in *Lasers—A Series of Advances., Vol. 4*, A. K. Levine and A. J. DeMaria, Eds. New York: Marcel Dekker, 1976, pp. 54-58.

[8] B. Zhou, T. J. Kane, G. J. Dixon, and R. L. Byer, "Efficient, frequency-stable diode laser-pumped Nd:YAG laser," *Opt. Lett.*, vol. 10, pp. 62-64, 1985.

[9] T. J. Kane, A. C. Nilsson, and R. L. Byer, "Frequency stability and offset locking of a laser-diode-pumped Nd:YAG monolithic nonplanar ring oscillator," *Opt. Lett.*, vol. 12, pp. 175-177, 1987.

[10] W. R. Trutna, Jr., D. K. Donald, and M. Nazarathy, "Unidirectional diode-laser-pumped Nd:YAG ring laser with a small magnetic field," *Opt. Lett.*, vol. 12, pp. 248-250, 1987.

[11] G. T. Forrest, "Diode-pumped solid-state lasers have become a mainstream technology," *Laser Focus/Electro-Optics*, vol. 23, pp. 62-74, 1987.

[12] C. L. Tang, H. Statz, and G. deMars, "Regular spiking and single-mode operation of ruby lasers," *Appl. Phys. Lett.*, vol. 2, pp. 222-224, 1963.

[13] A. R. Clobes and M. J. Brienza, "Single-frequency traveling-wave Nd:YAG lasers," *Appl. Phys. Lett.*, vol. 21, pp. 265-267, 1972.

[14] S. V. Kruzhalov, "Traveling-wave laser using the Faraday effect in an active field," *Sov. Phys. Tech. Phys.*, vol. 16, pp. 2081-2082, 1972.

[15] P. H. Lee and J. G. Atwood, "Measurement of saturation induced optical nonreciprocity in a ring laser plasma," *IEEE J. Quantum Electron.*, vol. QE-2, pp. 235-243, 1966.

[16] S. M. Jarrett and J. F. Young, "High-efficiency single-frequency cw ring dye laser," *Opt. Lett.*, vol. 4, pp. 176-178, 1979.

[17] T. F. Johnston, Jr. and W. Proffitt, "Design and performance of a broad-band optical diode to enforce one-direction traveling-wave operation of a ring laser," *IEEE J. Quantum Electron.*, vol. QE-16, pp. 483-488, 1980.

[18] J. A. Arnaud, "Degenerate optical cavities," *Appl. Opt.*, vol. 8, pp. 189-195, 1969.

[19] F. Biraben, "Efficacite des systemes unidirectionnels utilisables dans les lasers en anneau," *Opt. Commun.*, vol. 29, pp. 353-356, 1979.

[20] H. Statz, T. A. Dorschner, M. Holtz, and I. W. Smith, "The multioscillator ring laser gyroscope," in *Laser Handbook, Vol. 4*. M. L. Stitch and M. Bass, Eds. Amsterdam, The Netherlands: North-Holland, 1985.

[21] R. C. Jones, "A new calculus for the treatment of optical systems, I. Description and discussion of the calculus," *J. Opt. Soc. Amer.*, vol. 31, pp. 488-493, 1941.

[22] H. Hurwitz, Jr. and R. C. Jones, "A new calculus for the treatment of optical systems, II. Proof of three general equivalence theorems," *J. Opt. Soc. Amer.*, vol. 31, pp. 494-499, 1941.

[23] R. M. A. Azzam and N. M. Bashara, *Ellipsometry and Polarized Light*. Amsterdam, The Netherlands: North-Holland, 1987.

[24] H. de Lang, "Eigenstates of polarization in lasers," *Philips Res. Rep.*, vol. 19, pp. 429-440, 1964.

[25] ——, "Polarization properties of optical resonators passive and active," *Philips Res. Rep. Suppl.*, vol. 8, pp. 1-76, 1967.

[26] W. M. Doyle and M. B. White, "Properties of anisotropic Fabry-Perot resonator," *J. Opt. Soc. Amer.*, vol. 55, pp. 1221-1225, 1965.

[27] S. V. Kruzhalov, V. A. Parfenov, L. N. Pakhomov, and V. Y. Petrun'kin, "Optical isolators in YAG:Nd laser cavities," *Sov. Phys. Tech. Phys.*, vol. 30, pp. 1145-1147, 1985.

[28] V. Ya. Molchanov and G. V. Skrotskii, "Matrix method for the calculation of the polarization eigenstates of anisotropic optical resonators," *Sov. J. Quantum Electron.*, vol. 1, pp. 315-330, 1972.

[29] V. E. Sanders and R. M. Kiehn, "Dual-polarized ring lasers," *IEEE J. Quantum Electron.*, vol. QE-13, pp. 739-744, 1977.

[30] V. E. Sanders, "Polarization characteristics of an anisotropic ring laser," *Opt. Commun.*, vol. 29, pp. 227-229, 1979.

[31] V. I. Sardyko, "Polarization and frequency splitting of opposite waves in a ring laser with anisotropic resonator," *J. Appl. Spectrosc.* (USSR), vol. 30, pp. 39-46, 1979.

[32] A. P. Voitovich, A. A. Pavlyushchik, and S. V. Panteleev, "Phase-polarization method for control of the frequency spectrum of laser radiation," *Sov. J. Quantum Electron.*, vol. 7, pp. 21-25, 1977.

[33] J. M. Bennett and H. E. Bennett, "Polarization," in *Handbook of Optics*. Walter G. Driscoll, Ed. New York: McGraw-Hill, 1978, pp. 1-164.

[34] Ref. 23, pp. 272-273.

[35] M. Born and E. Wolf, *Principles of Optics*, 6th ed. Oxford: Pergamon, 1980, pp. 51-70.

[36] Ref. 23, p. 280.

[37] V. A. Zborovski and E. E. Fradkin, "Nonlinear interaction between differently polarized waves traveling in opposite directions in a ring laser," *Sov. Phys. JETP*, vol. 39, pp. 596-600, 1974.

[38] Ref. 23, p. 88.

[39] C. J. Buczek, R. J. Freiberg, and M. L. Skolnick, "Laser injection locking," *Proc. IEEE*, vol. 61, pp. 1411-1431, 1973.

[40] A. C. Nilsson, T. J. Kane, and R. L. Byer, "Monolithic nonplanar ring lasers; resistance to optical feedback," *Pulsed Single-Frequency Lasers: Technology and Applications*, W. K. Bischel, L. A. Rahn, Eds., Proc. SPIE, vol. 912, pp. 13-18, 1988.

[41] S. V. Kruzhalov and N. M. Kozhevnikov, "Polarization properties of a traveling-wave laser," *Sov. Phys. Tech. Phys.*, vol. 17, pp. 1156-1160, 1973.

[42] W. J. Press, B. P. Flannery, S. A. Teukolsky, and W. T. Vetterling, *Numerical Recipes*. Cambridge: Cambridge University, 1986, pp. 289-294.

[43] A. Owyoung and P. Esherick, "Stress-induced tuning of a diode-laser-excited monolithic Nd:YAG laser," *Opt. Lett.*, vol. 12, pp. 999-1001, 1987.

[44] J. J. Krebs, W. G. Maisch, G. A. Prinz, and D. W. Forester, "Applications of magneto-optics in ring laser gyroscopes," *IEEE Trans. Mag.*, vol. 16, pp. 1179-1184, 1980.

[45] A. L. Schawlow and C. H. Townes, "Infrared and optical masers," *Phys. Rev.*, vol. 112, pp. 1940-1949, 1958.

[46] S. F. Jacobs, "How monochromatic is laser light?," *Amer. J. Phys.*, vol. 47, pp. 597-601, 1979.

[47] S. V. Kruzhalov, V. A. Parfenov, L. N. Pakhomov, and V. Y. Petrun'kin, "Frequency stabilization of a Nd:YAG laser by means of $^{127}I_2$ absorption lines," *Sov. Tech. Phys. Lett.*, vol. 11, pp. 111-112, 1985.

[48] O. A. Orlov and V. I. Ustyugov, "Molecular cesium reference for frequency stabilization of a 1.06-μm Nd:YAG laser," *Sov. Tech. Phys. Lett.*, vol. 12, pp. 120-121, 1986.

[49] J. C. Bergquist, D. J. Wineland, W. M. Itano, H. Hemmati, H.-U. Daniel, and G. Leuchs, "Energy and radiative lifetime of the $5d^96s^2$ $^2D_{5/2}$ state in Hg II by Doppler-free two-photon laser spectroscopy," *Phys. Rev. Lett.*, vol. 55, pp. 1567-1570, 1985.

[50] W. W. Chow, J. B. Hambenne, T. J. Hutchings, V. E. Sanders, M. Sargent III, and M. O. Scully, "Multioscillator laser gyros," *IEEE J. Quantum Electron.*, vol. QE-16, pp. 918-936, 1980.

[51] W. W. Chow, J. Gea-Banacloche, and L. M. Pedrotti, "The ring laser gyro," *Rev. Mod. Phys.*, vol. 57, pp. 61-105, 1985.

[52] T. A. Dorschner, "Nonplanar rings for laser gyroscopes," *Fiber Optic and Laser Sensors, Proc. SPIE*, vol. 412, pp. 192-202, 1983.

[53] G. B. Jacobs, "CO_2 laser gyro," *Appl. Opt.*, vol. 10, pp. 219-220, 1971.
[54] ——, "CO_2 laser gyro using polarizationally isotropic cavity," *Appl. Opt.*, vol. 10, pp. 220-221, 1971.
[55] V. E. Sanders and D. Z. Anderson, "Isotropic nonplanar ring laser," U. S. Patent 4 247 832, 1981.
[56] S. P. Smyshlyaev, L. N. Kaptsov, K. N. Evtyukhov, and Y. D. Golyaev, "Rotating beams in a solid-state laser with a nonplanar ring cavity," *Sov. Tech. Phys. Lett.*, vol. 5, pp. 631-632, 1979.
[57] Y. D. Golyaev, K. N. Evtyukhov, and L. N. Kaptsov, "Uniaxial generation in YAG:Nd^{+3} continuous ring laser with nonplanar resonator," Moscow Univ. Phys. Bulletin, vol. 34, pp. 95-99, 1979.
[58] Y. D. Golyaev, K. N. Evtyukhov, L. N. Kapstov, and S. P. Smyshlyaev, "Spatial and polarization characteristics of radiation from a cw neodymium-doped garnet laser with a nonplanar ring resonator," *Sov. J. Quantum Electron.*, vol. 11, pp. 1421-1426, 1981.
[59] Y. D. Golyaev, K. N. Evtyukhov, L. N. Kapstov, and S. P. Smyshlyaev, "Temporal and spectral characteristics of radiation from a cw neodymium-doped garnet laser with a nonplanar ring resonator," *Sov. J. Quantum Electron.*, vol. 11, pp. 1427-1435, 1981.
[60] O. E. Nanii and A. N. Shelaev, "Magnetooptic effects in a YAG:Nd^{+3} ring laser with a nonplanar resonator," *Sov. J. Quantum Electron.*, vol. 14, pp. 638-642, 1984.
[61] G. B. Al'tshuler, E. D. Isyanova, V. B. Karasev, A. L. Levit, V. M. Ovchinnikov, and S. F. Sharlai, "Analysis of misalignment sensitivity of ring laser resonators," *Sov. J. Quantum Electron.*, vol. 7, pp. 857-859, 1977.
[62] E. F. Ischenko and E. F. Reshetin, "Analysis of the sensitivity of optical resonators to misalignment by the ray contour method," *J. Appl. Spectrosc.* (USSR), vol. 30, pp. 304-308, 1979.
[63] E. D. Isyanova, A. L. Levit, and V. M. Ovchinnikov, "Traveling-wave ring cavity with a nonplanar axis contour," *J. Appl. Spectrosc.* (USSR), vol. 36, pp. 287-291, 1982.
[64] A. L. Levit and V. M. Ovchinnikov, "Stability of a ring resonator with a nonplane axial contour," *J. Appl. Spectrosc.* (USSR), vol. 40, pp. 657-660, 1984.
[65] ——, "Dependence of the properties of an optical cavity on misadjustment," *Sov. J. Opt. Tech.*, vol. 50, pp. 423-425, 1984.
[66] I. I. Savel'ev and A. M. Khromykh, "Longitudinal modes of a cavity ring resonator," *Sov. J. Quantum Electron.*, vol. 6, pp. 821-826, 1976.
[67] I. W. Smith, "Optical resonator axis stability and instability from first principles," *Fiber Optic and Laser Sensors, Proc. SPIE*, vol. 412, pp. 203-206, 1983.
[68] L. A. Belousova, "Theory of Nonorthogonal Resonators," *J. Appl. Spectrosc.* (USSR), vol. 30, pp. 172-175, 1979.
[69] J. A. Arnaud and H. Kogelnik, "Gaussian light beams with general astigmatism," *Appl. Opt.*, vol. 8, pp. 1687-1693, 1969.
[70] C. G. B. Garrett, "Normal modes of a ferromagnetic laser with one Brewster face," *IEEE J. Quantum Electron.*, vol. QE-3, pp. 139-142, 1967.

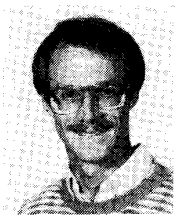

Alan C. Nilsson was born in Los Alamos, NM, in 1957. He received the B.A. degree in mathematics and physics from the University of California, San Diego, in 1980 and the M.S. degree in applied physics from Stanford University, Stanford, CA, in 1983.

He is currently working towards the Ph.D. degree in applied physics. His dissertation research at Stanford has emphasized modeling, development, and heterodyne characterization of narrow linewidth, diode-laser-pumped, monolithic nonplanar ring lasers.

Mr. Nilsson is a member of the American Physical Society and the Optical Society of America.

Eric K. Gustafson was born in Fairbanks, AK, in 1951. He received the B.A. degree in physics from the California Institute of Technology, Pasadena, CA, in 1974 and the M.S. and Ph.D. degrees in applied physics from Stanford University, Stanford, CA. His dissertation work involved high-resolution nonlinear spectroscopy in supersonic expansions.

He was a Research Physicist with the Space Sciences Laboratory at the University of California, Berkeley, from 1983 to 1985, where he conducted research on fast, far-infrared photoconductors for use in astronomical heterodyne receivers. He is currently a Research Associate in the Edward L. Ginzton Laboratory at Stanford University and is involved in research on miniature, all-solid-state ring lasers and their applications in high resolution spectroscopy and as pump sources for optical parametric oscillators.

Robert L. Byer (M'75—SM-83-F'87) received the Ph.D. degree in applied physics from Stanford University, Stanford, CA, in 1969.

After joining the Applied Physics Department at Stanford in 1969, he began research in remote sensing using tunable laser sources. Research in that area led to the development of the unstable resonator Nd:YAG laser and to high-power, tunable infrared generation in $LiNbO_3$ parametric oscillators. In 1974 he and his colleagues initiated research in coherent anti-Stokes Raman spectroscopy (CARS), named the effect, and extended the research to high resolution, CW CARS spectroscopy in supersonic flows. In 1976 he suggested the use of stimulated Raman scattering in hydrogen gas as a means of generating 16 μm radiation from a CO_2 laser source. Research at Stanford confirmed the expected efficiency of the approach. Research in high-peak and average-power slab geometry solid-state lasers began in 1980. The program led to theoretical and experimental progress in advanced solid-state laser sources. Recent research has centered on diode-pumped solid-state laser sources and their applications. His early and continuing interest has been in nonlinear optics and the applications of nonlinear processes to unique measurements. At Stanford University, he served as Chairman of the Applied Physics Department from 1981 to 1984 and as Associate Dean of Humanities and Sciences from 1984 to 1987. Currently, he is Vice Provost and Dean of Research at Stanford University. He helped found Quanta Ray Inc. in 1975 and Lightwave Electronics Corporation in 1984. He has published more than 190 technical papers and holds 19 patents in the field of nonlinear optics and laser devices.

Dr. Byer is a member of the National Academy of Engineering and a Fellow of the Optical Society of America. He was president of the IEEE Lasers and Electrooptics Society in 1985.